STANDARDIZATION AND APPLICATION OF A SPECTROPHOTOMETRIC METHOD FOR REDUCTIVE CAPACITY MEASUREMENT OF NANOMATERIALS

A Thesis

by

WONJOONG HWANG

Submitted to the Office of Graduate Studies of
Texas A&M University
in partial fulfillment of the requirements for the degree of

MASTER OF SCIENCE

August 2010

Major Subject: Mechanical Engineering

STANDARDIZATION AND APPLICATION OF A SPECTROPHOTOMETRIC METHOD FOR REDUCTIVE CAPACITY MEASUREMENT OF NANOMATERIALS

A Thesis

by

WONJOONG HWANG

Submitted to the Office of Graduate Studies of
Texas A&M University
in partial fulfillment of the requirements for the degree of

MASTER OF SCIENCE

Approved by:

Chair of Committee,	Bing Guo
Committee Members,	Ramesh Talreja
	Xinghang Zhang
Head of Department,	Dennis O'Neal

August 2010

Major Subject: Mechanical Engineering

ABSTRACT

Standardization and Application of Spectrophotometric Method for Reductive Capacity Measurement of Nanomaterials. (August 2010)

Wonjoong Hwang, B.E., Korea Military Academy

Chair of Advisory Committee: Dr. Bing Guo

In this study, a reproducible spectrophotometric method was established and applied to measure reductive capacity of various nanomaterials. Reductive capacity had been implicated in the toxicity of nanomaterials, but a standardized measurement method had been lacking until this work.

The reductive capacity of nanoparticles was defined as the mass of iron reduced from Fe^{3+} to Fe^{2+} by unit mass of nanoparticles, in an aqueous solution that initially contained ferric ions. To measure the reductive capacity, the nanomaterials were incubated in a ferric aqueous solution for 16 hours at 37 ˚C, and the reductive capacity of the nanoparticles was determined by measuring the amount of Fe^{3+} reduced to Fe^{2+} using a spectrophotometric method. The reagents 1,10-phenanthroline and hydroquinone were used as a Fe^{2+} indicator and a reducing agent respectively for the assay.

To standardize this method, various experiments were carried out. For the initial ferric solution, various Fe salts were tested, and Iron(III) sulfate was chosen as Fe salt for the standard method. The measured reductive capacity of nanoparticles was found to vary with the measurement conditions; the measured reductive capacity increased with

increasing the Fe/nanoparticle ratio; the measured reductive capacity increased with incubation time and leveled off after 8 hours of incubation. For hydrophobic materials, the surfactant Tween-20 was added so that the particles could be wetted and suspended in the ferric aqueous solution. After incubation, the particles were removed from the solution by either filtration or centrifugation before applying the spectrophotometric method. In addition, optimal pH and minimum time to reach ultimate color intensity were also found.

Carbon-based nanomaterials, standard reference material and metal oxides were measured for their reductive capacities with this method and characterized by transmission electron microscopy (TEM), energy dispersive x-ray spectroscopy (EDS), x-ray diffraction (XRD), BET measurement and Raman spectroscopy. For some nanoparticles, the reductive capacity was measured for both the pristine form and the form treated by oxidization or grinding.

All carbon-based nanomaterials, except for pristine C60, have a significant reductive capacity while reductive capacity of metal oxides is very low. And it was found that reductive capacity can be increased by surface functional groups or structural defects and reduced by oxidization or heating (graphitization). The reductive capacity of a material can play an important role in its toxicology by synergistic toxic effects in the presence of transition metal ions through the Fenton reaction. Moreover, even without transition metal ions, the ability of a material to donate electrons can be involved in toxicity mechanisms via generation of reactive oxygen species.

DEDICATION

To my lovely wife, Eunsun, precious daughter, Ashely, and all of my family members who have always been there for me

ACKNOWLEDGEMENTS

I would like to thank my advisor, Dr. Bing Guo, not only for academic guidance and advice but also for the support he has given me in last two years. Sincere thanks are due to Dr. Ramesh Talreja and Dr. Xinghang Zhang for their valuable recommendations and consideration as committee members.

I also appreciate the big favors from Mike Berg and Dr. Sayes of doing sample preparation and BET measurements. I would like to thank Wonchang Park for doing Raman analysis and Dr. King, in the Aerosol Technology Lab, for providing various instruments in the lab. I also want to extend my gratitude to group members, Gagan Singh and Chunghoon Lee, who have given great help.

TABLE OF CONTENTS

Page

LIST OF FIGURES

FIGURE Page

LIST OF TABLES

1. INTRODUCTION

Spectrophotometry is essentially a trace analysis technique and is widely used due to its selectivity, accuracy, rapidity, low cost and ease of operation. Using various colorimetric chelating reagents that form a complex and absorb light, it has been developed as a way to determine metal ions [1-7], inorganic compounds [8-11] and organic compounds [12-20]. This method also offers a way for detection and speciation of Fe ions [21-25], and Fe determination and speciation techniques using spectrophotometric method were also applied to detect other substances [26-30] or to measure reactivity of materials [31, 32]. Toxicology studies have also used spectrophotometric method with different detection or determination techniques [33-37].

Most of the toxicology mechanisms are related to redox reactions, and generation of reactive oxygen species (ROS) is known as one of main culprits for toxicity of materials [38]. Hydroxyl radical ($OH^{\cdot}$), one of strongest ROS, can be generated by following Fenton reaction [39]:

$$Fe^{2+} + H_2O_2 \rightarrow Fe^{3+} + OH^{\cdot} + OH^{-\cdot}$$

In this regards, the ability of a material to reduce Fe^{3+} to Fe^{2+} ions may be directly related to its toxicity via redox cycling [39-41]. Therefore, there is a need to characterize nanomateirals for their reductive capability towards Fe^{3+}, for assessing the

---

This thesis follows the style of *Environmental Toxicology and Chemistry*.

toxicity of nanomateirals. The reductive capacity of a material is defined as the mass of Fe^{3+} that can be reduced to Fe^{2+} by unit mass of nanomaterial:

$$\text{Reductive capacity} = \frac{\text{Mass of reduced } Fe^{3+} \text{ ions}}{\text{Mass of used material}} (\text{g/g}).$$

Even if a huge number of toxicology studies have been carried out, there is no practical way to compare a result with other studies because the results obtained from each toxicology study are not comparable unless experiments were performed in exactly the same way. Besides, *in vivo* experiments of toxicity of a material requires relatively a long period of time from a few days to several years [42-44], and *in vitro* experimental designs tend to be complicated to satisfy desired conditions.

This study was motivated to establish a simple reproducible method to measure the reductive capacity of nanomaterials, giving ease of operation and comparison. The aim of this study is to standardize and validate the spectrophotometric method for reductive capacity measurement, which can be applicable for different types of materials, and present reductive capacities of carbon nanoparticles and nanotubes, metal oxides and standard reference materials to find out the relation between reductive capacity results and toxicity of materials.

2. THEORY

2.1 1,10-Phenanthroline and Ferroin

1,-10-Phenanthroline (Phen) is a polycylclic organic compound composed of three benzene rings with two nitrogen atoms, and its molecular formula is $C_{12}H_8N_2$. 1,10-phenanthroline forms a complex called 'ferroin' with Fe^{2+} by the following reaction.

$$Fe^{2+} + 3Phen \rightarrow [Fe(Phen)_3]^{2+}, E^o = 1.06V$$

The structure of 1,10-phenanthroline and ferroin are shown in Fig. 1.

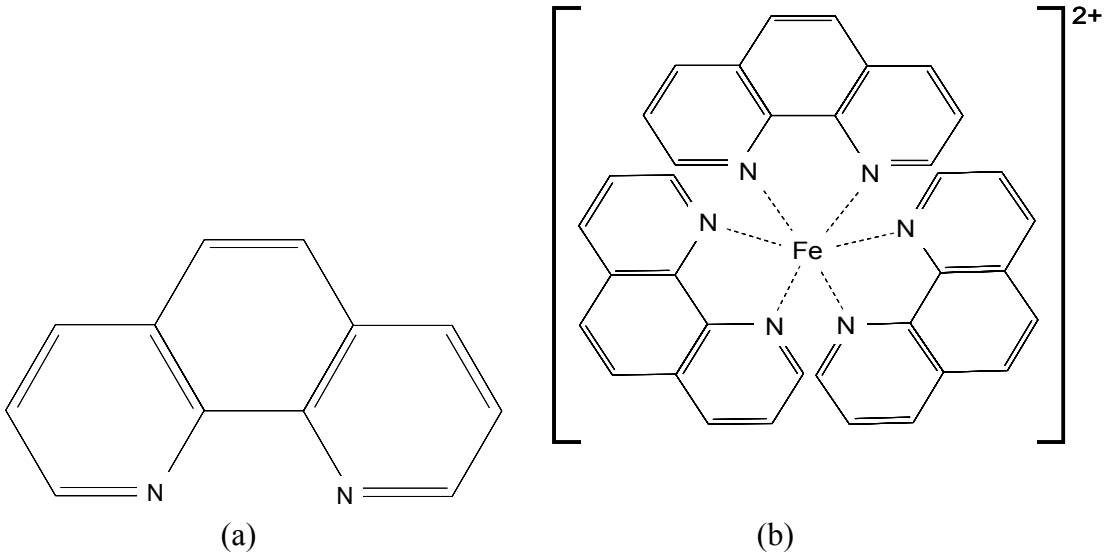

Fig. 1. The structures of (a) 1,10-phenanthroline[a] and (b) Ferroin.
[a]'1,10' indicates location of nitrogen atoms.

Ferroin, which appears in red, plays the role of absorbing species in an aqueous solution with a maximum molar absorptivity of 11,100 $M^{-1}cm^{-1}$ at 510 nm [45]. Thus, 1,10-phenanthroline has been used as an indicator of Fe^{2+} ion with aid of a spectrophotometer.

2.2 Absorbance and Spectrophotometer

The Beer-Lambert law states the relation between the absorption of light and properties of the absorber. For liquids, the transmission (T) and absorbance (A) are defined as

$$T = \frac{I}{I_0} = 10^{-\varepsilon lc} \tag{1}$$

$$A = -\log_{10}\left(\frac{I}{I_0}\right) \tag{2}$$

where I_0 and I are the intensity of the light before and after passing through the absorber respectively as shown in Fig. 2. ε is the molar absorptivity, and l and c is the path length of the light and the concentration of absorbing species, respectively. Based on these two equations, a relation between absorbance (A) and the concentration of absorbing species (c) can be obtained as

$$A = -\log_{10}\left(\frac{I}{I_0}\right) = \varepsilon lc \tag{3}$$

Equation (3) indicates if absorbance of a substance with the same molar absorptivity (ε) is measured with fixed path length (l) and wavelength, the result will be

proportional to the concentration of absorbing species (*c*). However, it should be noted that Beer's law cannot be applied to very high concentrations of absorbing species and suspensions of particles [46].

An illustration of the absorbance measurement by a single-beam spectrophotometer is shown in Fig. 2.

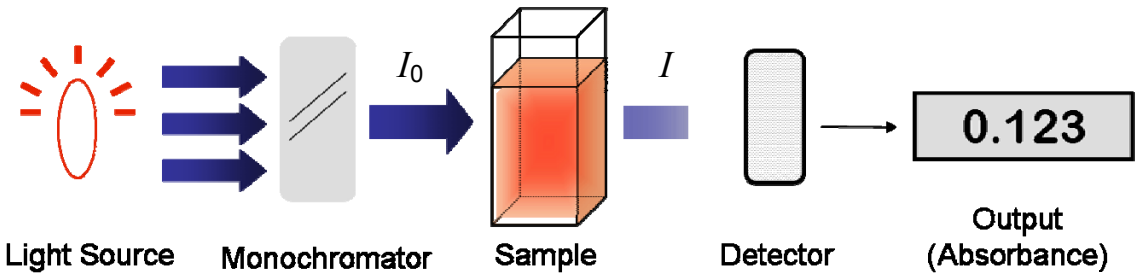

Fig. 2. An illustration of the absorbance measurement.

2.3 Hydroquinone

Hydroquinone is a heterocyclic organic compound with two hydroxyl groups (-OH) bonded to a phenyl ring, having the chemical formula of $C_6H_4(OH)_2$. It can be converted to benzoquinone by oxidization producing two electrons as seen in Fig. 3.

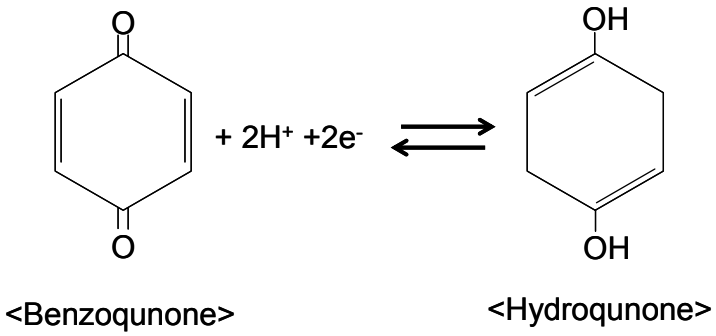

Fig. 3. Reduction and oxidation equilibria of hydroquinone.

In the presence of Fe^{3+}, hydroquinone donates electrons and reduces Fe^{3+} to Fe^{2+} by the following reaction.

$$2Fe^{3+} + C_6H_4(OH)_2 \rightarrow 2Fe^{2+} + C_6H_4O_2 + 2H^+ , E^o = 0.071V \text{ [47]}$$

Having a positive redox potential of the reaction, the reduction of Fe^{3+} by hydroquinone takes place spontaneously until either Fe^{3+} or hydroquinone is all consumed.

3. METHODOLOGY FOR REDUCTIVE CAPACITY ANALYSIS

All chemicals used in this study are of reagent grade or better, and de-ionized (DI) water was obtained via a Millipore Milli-Q and Milli-RO Ultrapure Water Purification System. Glassware and laboratory tools were cleaned by sonication, rinsed with DI water and dried in the ambient air before use. All preparations and experiments were conducted at room temperature kept at 20 ± 3 ˚C except for incubation. The reductive capacity was determined from a set of three replicates, and absorbance was measured at least three times for each sample at 512 nm.

3.1 Equipment for Reductive Capacity Measurement

The single-beam 1100 series Spectrophotometer (Cole Parmer, Vernon Hills, IL) was used to read absorbance of the solutions in a 4.5 ml optical polystyrene cuvette (58017-880, VWR, West Chaser, PA). A 10 L analog water bath (Cole Parmer, Vernon Hills, IL) was used for incubation of the samples. A Model 5804 centrifuge (Eppendorf, Westbury, NY) was used for centrifugation of incubated solutions in 50 ml polypropylene concial tubes (Becton Dickinson Labware, Franklin Lakes, NJ), and 9 cm (diameter) grade 415 paper filters (28320-041, VWR, West Chaser, PA) were used for filtration of incubated solutions. An electronic balance (ZSA80, Scientech, Boulder, CO) and pH meter (Extech, Waltham, MA) was used to measure mass and pH respectively. 5, 10 and 25 ml of polystyrene pipettes (Becton Dickinson Labware, Franklin Lakes, NJ)

and micropipettes with range of 40 ~ 200 μl and 200 ~ 1000 μl (Cole Parmer, Vernon Hills, IL) were used for dispensing adequate quantities of liquids. An ultrasonic cleaner (Model T50, VWR, West Chaser, PA) was used for cleaning glassware and dispersing particles in suspensions. Mortar and pestle (Cole Parmer, Vernon Hills, IL) were used to generate structural defects of carbon nanotubes by grinding, and a flame synthesis apparatus was used in synthesis of Soot-A, TiO_2 and Fe_2O_3.

3.2 Calibration Curve

A relation between Fe^{2+} concentration and absorbance was obtained by a calibration curve of a series of absorbance measurements with known Fe^{2+} concentration. A stock solution for calibration curve was prepared by dissolving 10.7 mg of Iron(III) sulfate hydrate ($Fe_2(SO_4)_3 \cdot xH_2O$, Reagent grade, Alfa Aesar, Ward Hill, MA) in 1L of DI water. The x value in the chemical formula was revealed to be 6.08 by the manufacturer. Different amounts of the stock solution; none, 5, 10, 20, 30 and 50 ml, were pipetted into 100 ml volumetric flasks so that each flask had various Fe ion concentrations ranging from 0 ~ 1.2 mg/L. A 1-ml solution containing 1w% hydroquinone ($C_6H_4(OH)_2$, 99 %, Alfa Aesar, Ward Hill, MA) solution was added to reduce Fe^{3+} to Fe^{2+} ions, and 0.25 ml of 20 % sulfuric acid (H_2SO_4, 95 %, Labchem, Pittsburgh, PA) was then added to make the solution low pH around 2. Finally, 10 ml of 0.3w% 1,10-phenanthroline ($C_{12}H_8N_2$, >99 %, Alfa Aesar, Ward Hill, MA) which was prepared by dissolving 0.6 g of 1,10-phenanthroline in 20 ml of acetone (C_3H_6O,

>99.5 %, Sigma-Aldrich, St. Louis, MO) and diluted to 200 ml with DI water, was added to form ferroins with Fe^{2+} ions in the solution, making a red color with varied intensities according to the Fe^{2+} concentration in the solution. The sequence of addition and quantities of stock solution and chemicals used in each flask are shown in Table 1.

Table 1. The sequence and quantities of the stock solution and reagents for calibration curve.

Flask No.	(1)	(2)	(3)	(4)	(5)	(6)	Sequence
Stock solution	·	5 ml	10 ml	20 ml	30 ml	50 ml	1
1 % Hydroquinone	1ml						2
20 % sulfuric acid	0.25 ml						3
0.3 % Phenanthroline	10 ml						4

The pH of final solutions for absorbance reading was within 2 ± 0.1, and absorbance measurements of each solution were performed 1 hour after the solution was made. The results are plotted in Fig. 4. Absorbance and Fe^{2+} ion concentration (mg/L) has a linear relationship with slope of 0.1893.

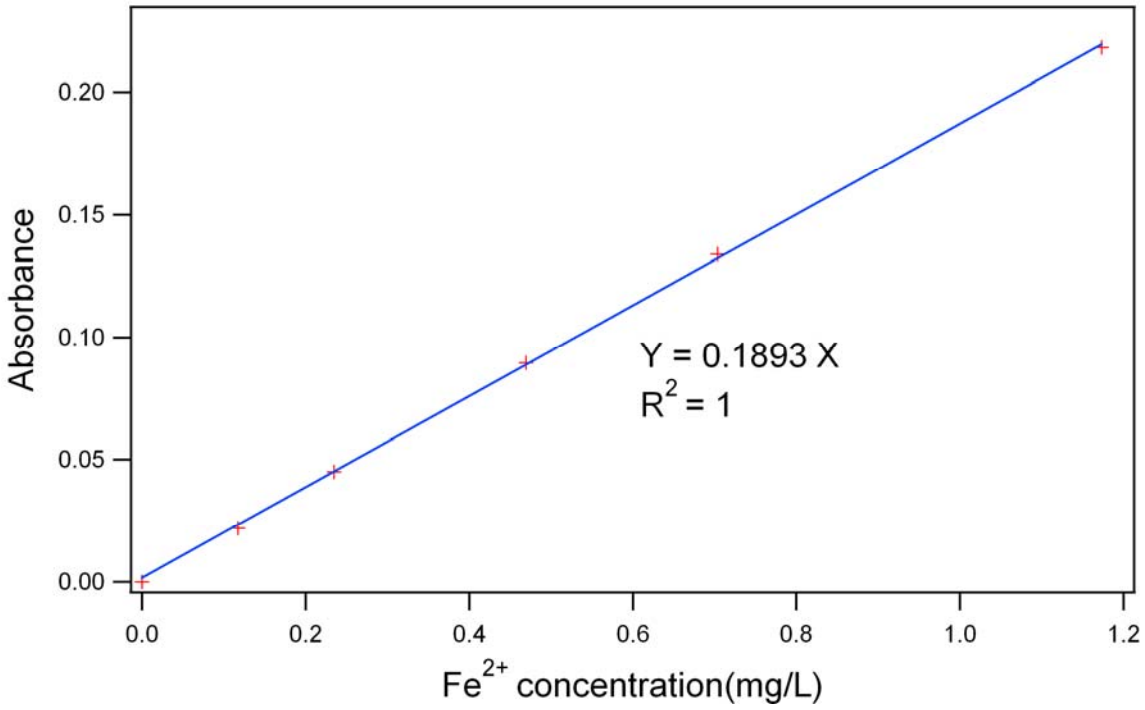

Fig. 4. Calibration curve of $Fe_2(SO_4)_3$ at pH 2

3.3 Reductive Capacity Measurements

Solution Preparations for Incubation

The samples were prepared for each reductive capacity measurement in the following steps:

(1) Three replicate samples: To each of three replicate 200-ml beakers, the salt $Fe_2(SO_4)_3$ 9.0 ± 0.2 mg and the nanomaterial 30 ± 0.2 mg were added. If the nanomaterial was hydrophobic, 2 ml of 0.12 mM surfactant (Tween 20, Bio-Rad, Hercules, CA) was added to the sample so that it could be wetted by water.

(2) One reference sample: To a fourth 200-ml beaker, the nanomaterial 30 ± 0.2mg was added.

(3) DI water in the amount of 75 ml was then added into each beaker, and the beakers were sealed with Parafilm® (Pechiney Plastic Packing, Chicago, IL).

(4) The solutions were gently shaken by hand before incubation.

Incubation and Particle Separation

The water bath was warmed up before use and set at 37 ˚C to mimic human body conditions. The solutions containing both Fe^{3+} ions and nanomaterials were placed in a water bath which was kept at 37 ± 3 ˚C. The nanomaterials were allowed to react with Fe^{3+} ions in aqueous solutions for 16 hours. After 16 hours of incubation, solutions were

decanted to 100ml volumetric flasks by being passed through a paper filter so the particles were separated from the solution. And the particle-free solutions in the flasks were diluted to the 100 ml mark with DI water. If the nanomaterials could not be filtered by a paper filter, the particles were separated using a centrifuge. The incubated solutions were directly decanted into 100 ml volumetric flasks and diluted to 100 ml with DI water and transferred into two 50 ml centrifuge vials. The vials were centrifuged for 8 minutes at 4000 revolutions per minute (rpm), and as a result, particles were precipitated on the bottom of the vials. The supernatants in the two vials were pipetted together into another 200 ml beaker, and thus, particle-free solutions were obtained.

Color Development and Absorbance Measurements

From each particle-free solution, three 25-mL aliquots were taken and put into three 100 ml volumetric flasks. These flasks were labeled A, B and C respectively for identification. To 'B' flask, 1 ml of 1 % hydroquinone was added as a reducing agent to reduce remaining Fe^{3+} to Fe^{2+}, followed by addition of 0.25 ml of 20 % of sulfuric acid into all of three flasks. And then, 10ml of 0.3% 1,10-phenanthroline was added to 'B' and 'C' flasks to develop color. The quantities of chemicals added in each flask are shown in Table 2.

Table 2. The quantities of reagents added in final solutions.

Flask ID.	A (Method Blank)	B (Fe total)	C (Fe^{2+})
Particle-Free Solution	25 ml	25 ml	25 ml
1% hydroquinone	·	1 ml	·
20% sulfuric acid	0.25 ml	0.25 ml	0.25 ml
0.3% phenanthroline	·	10 ml	10 ml

After adding 1,10-phenanthroline, each solution was diluted to 100 ml with DI water and flipped over several times to mix the chemicals. After allowing the solutions no less than 1 hour to finish developing its color, 2~3 ml of solution was transferred to the cuvette, and absorbance was measured by a spectrophotometer at wavelength 512 nm. Before each measurement, absorbance of DI water was set to zero, and the cuvette was rinsed with the solution to be measured. Flask 'A' represents a absorbance background affected only by its own color or remaining particles in solution not by Fe ions. Absorbance difference of flasks 'B' and 'C' from flask 'A' indicate total Fe (sum of Fe^{3+} and Fe^{2+}) ions and Fe^{2+} ion concentration in the solutions respectively.

Calculation of Mass of Reduced Fe^{2+} and Reductive Capacity

Absorbance of Fe^{2+} (Flask 'C') subtracted by absorbance of method blank (Flask 'A') indicates intensity of color solely due to Fe^{2+}. The difference of absorbance between Fe^{2+} and method blank was compared to that of calibration curve, and thus the corresponding Fe^{2+} ions concentration (mg/L) in the solution could be found. Since neither Fe^{2+} ions exist in initial $Fe_2(SO_4)_3$ aqueous solution, nor Fe^{3+} ions are reduced by

themselves without reducing agent, existing Fe^{2+} ions should be attributed to reduction of Fe^{3+} by co-incubated materials. Once the concentration of Fe^{2+} ions (mg/L) is obtained by comparison of absorbance results and calibration curve, a mass of reduced Fe^{3+} to Fe^{2+} during incubation could be calculated based on the procedure of the final solutions preparation. To get the reductive capacity of a material, reduced Fe^{3+} mass was divided by mass of nanomaterials used. The mean of reductive capacity results from triplicate samples was used as the reductive capacity of the nanomaterials. If a material contains a detectable amount of Fe^{2+} soluble in aqueous solutions of the same condition with incubation, the extractable Fe^{2+} per unit mass of sample (g/g) should be investigated as described in appendix C and taken into account in calculation of reductive capacity by subtracting extracted Fe^{2+} from calculated Fe^{2+} based on the absorbances.

Entire procedures of the reductive capacity measurement of single sample are shown as a flow chart in Fig. 5.

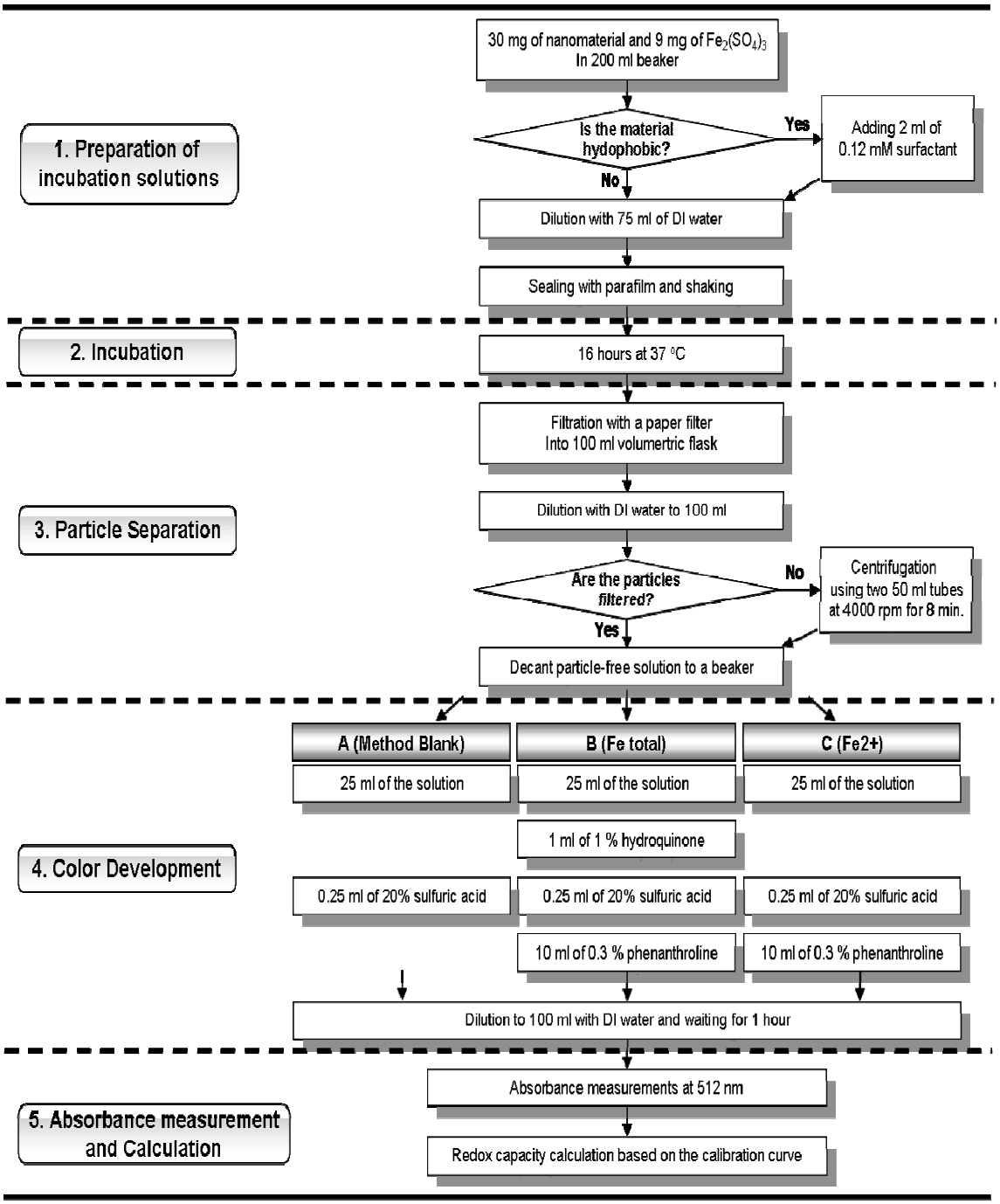

Fig. 5. A flow chart of the reductive capacity measurement.

3.4 Characterization of Nanomaterials

The examined materials were characterized using XRD, TEM, EDS, Raman Spectroscopy and BET analysis.

To analyze crystalline structure of flame synthesized TiO_2, the collected particles on alumina filter (Whatman, Maidstone, England) was directly placed on the sample holder and determined by Bruker-AXS D8 Powder X-ray diffractometer (Bruker, Madison, WI) with Cu source.

The morphology and shape of nanomaterials were charaterized by TEM images. The nanomaterials were suspended in isopropyl alcohol ($C_3H_7(OH)$, 99.5 %, Mallinchrodt Baker, Phillipsburg, NJ) and sonicated. Drops of the suspensions were put on various types of copper grid (Ted Pella Inc., CA); Type-B carbon film support for metal oxide, Type-A silicon monoxide and holey carbon support film for carbon nanoparticles and nanotubes. After evaporation of isopropyl alcohol, nanomaterials were remained and deposited on the copper grids. JEOL 2010 microscope (Jeol Ltd., Tokyo, Japan) was operated at 200kV, and TEM images were obtained by a Gatan ORIUS CCD camera (Gatan Inc., Pleasanton, CA). Energy dispersive X-ray spectroscopy (EDS) analysis was also performed along with TEM to confirm impurities in the materials.

Raman spectroscopy was used to detect structural defects and graphitization of CNTs. CNTs were placed on glass slides, and Raman spectra of CNTs were obtained by Horiba Jobin-Yvon Labram Raman confocal Microscope 341-K (Horiba Ltd, Kyoto, Japan) using 633 nm laser.

BET measurements were carried out to determine specific surface area of the materials. Prior to the surface area measurement, density of each material was measured on a Micrometeitics Pynometer with a 0.1 cc insert using helium gas. And surface area was then measured on a Micromeritics ASAP 2020 under nitrogen absorption.

3.5 Statistical Analysis

Analysis of variation (ANOVA) and Student's *t*-test were used for statistical analysis of the reductive capacity results. Basically, the reductive capacity results, obtained from triplicates, were compared using these statistical tools to see if reductive capacity of a material is significantly different from that of others. Difference within a group of more than three materials was assessed by One-way ANOVA with a significance level of 0.05 ($\alpha = 0.05$), and a paired two-sample *t*-test was used with 0.05 of probability ($P<0.05$) to tell the significance of the reductive capacity difference before and after treatments. All the results were expressed as mean ± standard deviation.

4. REDUCTIVE CAPACITY OF NANOMATERIALS

4.1 Overview of Materials

Carbon Nanomaterials

Carbon black (CB), carbon nanotubes (CNTs), fullerenes (C_{60}) were purchased from commercial companies, and soot particles were generated using acetylene (Soot-A) as identified in Table 3 with detailed information of the materials. In addition, some of these materials were modified through treatments; CNTs were ground by a mortar and pestle and aged in ambient air, and CB and Soot-A were oxidized in DI water for 2 weeks as described in appendix A. The representative TEM images of carbon nanomaterials are shown in Fig. 6.

Table 3. Sample information of carbon nanoparticles and nanotubes.

Sample ID	Materials	Characteristics	Id # CAS/Lot	Manufacturer
CB	Carbon Black (Printex 90)	Diameter : 5 - 30 nm (Mean : 14 nm)	C1333-86-4	Degussa
Soot-A	Soot generated from Acetylene	·	N/A	N/A
SCNT_1	Single-wall carbon nanotubes	Outer Diameter : 1-2 nm Length : 5-30 μm	Sku-0101	Cheap Tubes
SCNT_2	Single-wall carbon nanotubes with OH groups	Outer Diameter : 1-2 nm Length : 10-30 μm	Sku-0102	Cheap Tubes
SCNT_3	Single-wall carbon nanotubes with COOH groups	Outer Diameter : 1-2 nm Length : 5-30 μm	Sku-0103	Cheap Tubes
C_{60}	Refined Mixed Fullerenes	Outer diameter : 1 nm	C99685 -96-8	MER
$C_{60}OH$	$C_{60}(OH)_x(ONa)_y$ ($y \approx 6\sim8$, $x+y \approx 24$)	·	N/A	MER
$C_{60}H$	$C_{60}H_x$ ($x \approx 33$)	·	N/A	MER
MCNT_1	Multi-wall carbon nanotubes	Outer Diameter : < 8 nm Length : 10-30 μm	Sku-030101	Cheap Tubes
MCNT_2	Multi-wall carbon nanotubes	Outer Diameter : 10-20 nm Length : 10-30 μm	Sku-030103	Cheap Tubes
MCNT_3	Multi-wall carbon nanotubes	Outer Diameter : > 50 nm Length : 10-20 μm	Sku-030107	Cheap Tubes
MCNT_4	Graphitized MCNT_2	Outer Diameter : 10-20 nm Length : 10-30 μm	Sku-030103	Cheap Tubes
MCNT_5	Graphitized MCNT_3	Outer Diameter : > 50 nm Length : 10-20 μm	Sku-030107	Cheap Tubes

Fig. 6 shows representative TEM images of carbon nanoparticles and nanotubes.

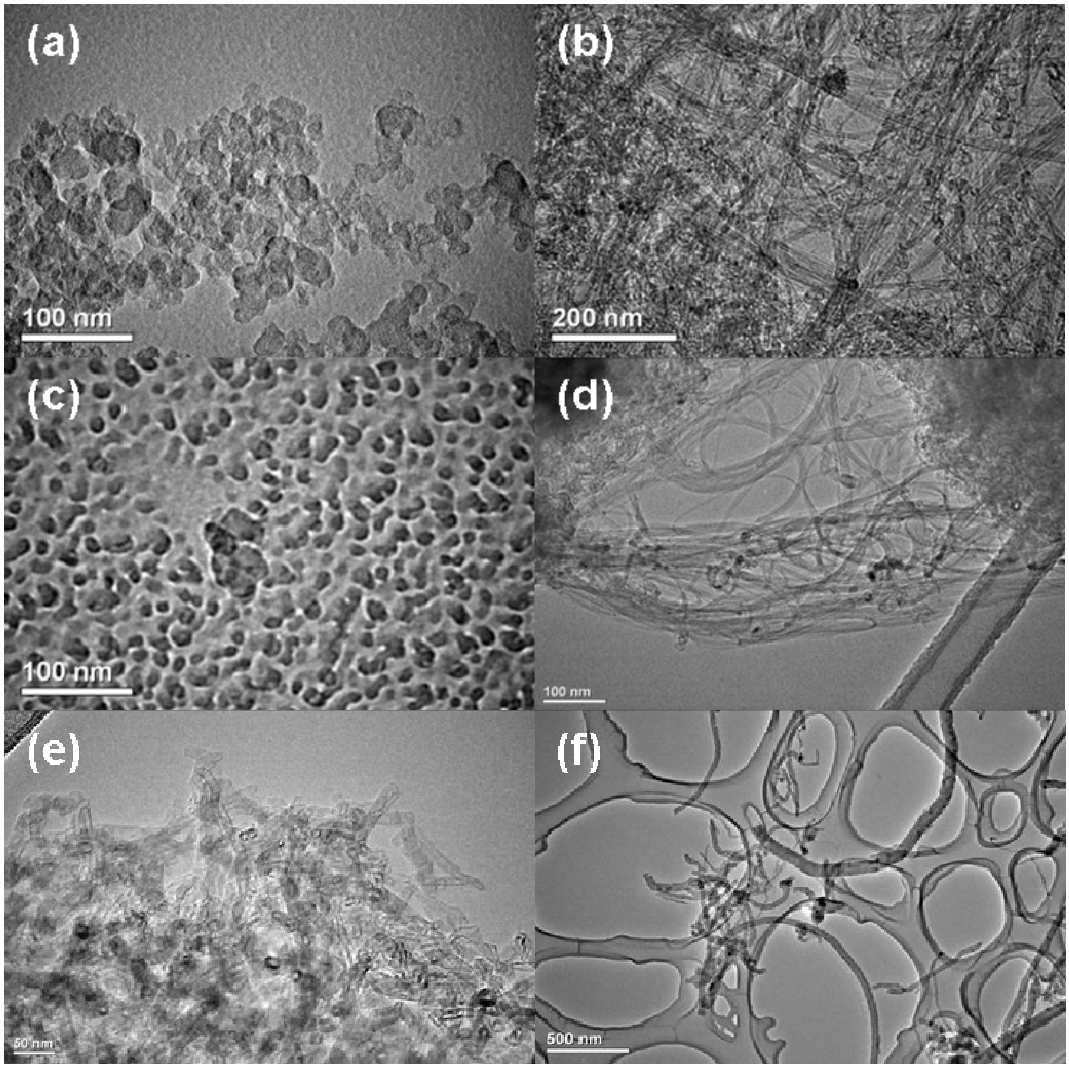

Fig. 6. Representative TEM images of carbon nanoparticles and nanotubes. (a) Carbon black (CB), (b) Single-wall carbon nanotubes (SCNT_1), (c) Fullerenes (C_{60}), (d) Multi-wall carbon nanotubes (MCNT_1), (e) Graphitized carbon nanotubes (MCNT_4), (f) Ground MCNT_3.

Metal Oxides

Commercially available titanium oxides (TiO_2), Silicon(IV) oxide, MIN-U-SIL 5 Crystalline silica and CAB-O-SIL M-5 amorphous silica were purchased from commercial companies as shown in Table 4. TiO_2 nanoparticles were generated through flame synthesis as described in appendix B, and its crystal structure was turned out to be pure anatase as shown in Fig. 7. The representative TEM images of metal oxides are shown in Fig. 8.

Table 4. Sample information of metal oxides.

Sample ID	Materials	Purity / Size	CAS/Lot #	Manufacturer
Ti-A	Commercial TiO_2 (Anatase)	99.6 %, Diameter : 20-200 nm	I22J02	Alfa Aesar
Ti-S	Synthesized TiO_2 (Anatase)	N/A , Diameter : 20-200 nm	N/A	Synthesized in Lab
Ti-R	Commercial TiO_2 (Rutile)	99.99 %, N/A	A29T003	Alfa Aesar
Si-C	MIN-U-SIL 5 Crystalline Silica	> 99%, N/A	08041309	U.S. Silica
Si-A	CAB-O-SIL M-5 Amorphous Silica	> 99.9 % Diameter : 5-30 nm	969702	CABOT
Si-S	Silicon(IV) oxide (SiO_2)	100 %, N/A	H30S013	Alfa Aesar

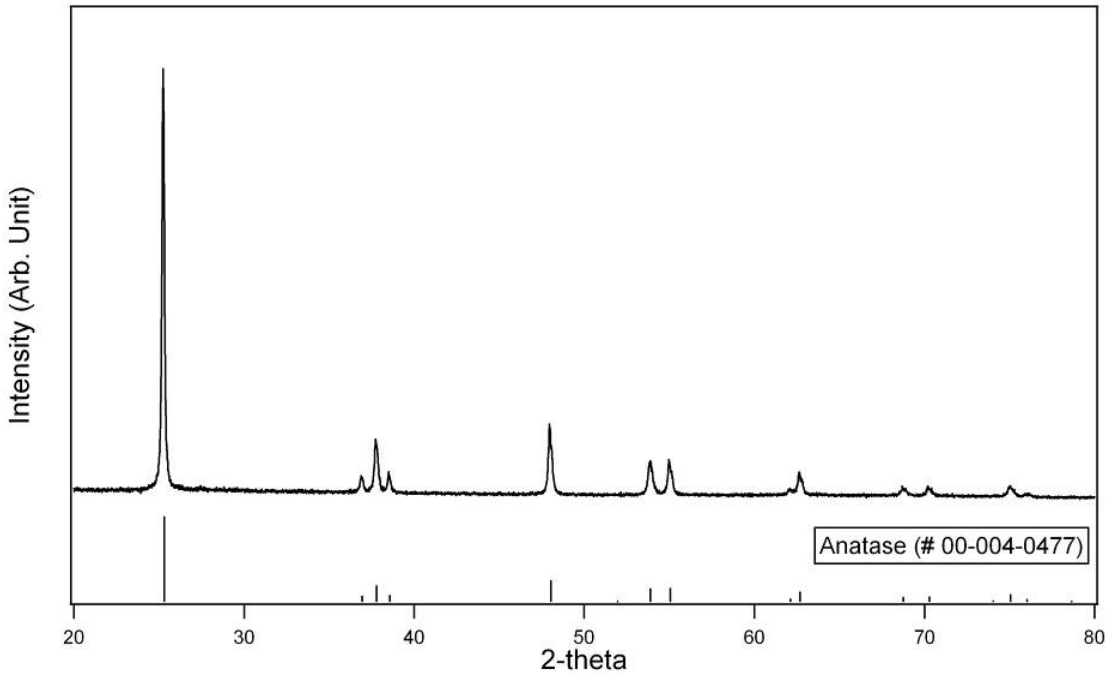

Fig. 7. XRD pattern of synthesized TiO_2. It shows the flame synthesized TiO_2 has pure anatase phase.

Representative TEM images of metal oxides are shown in Fig. 8.

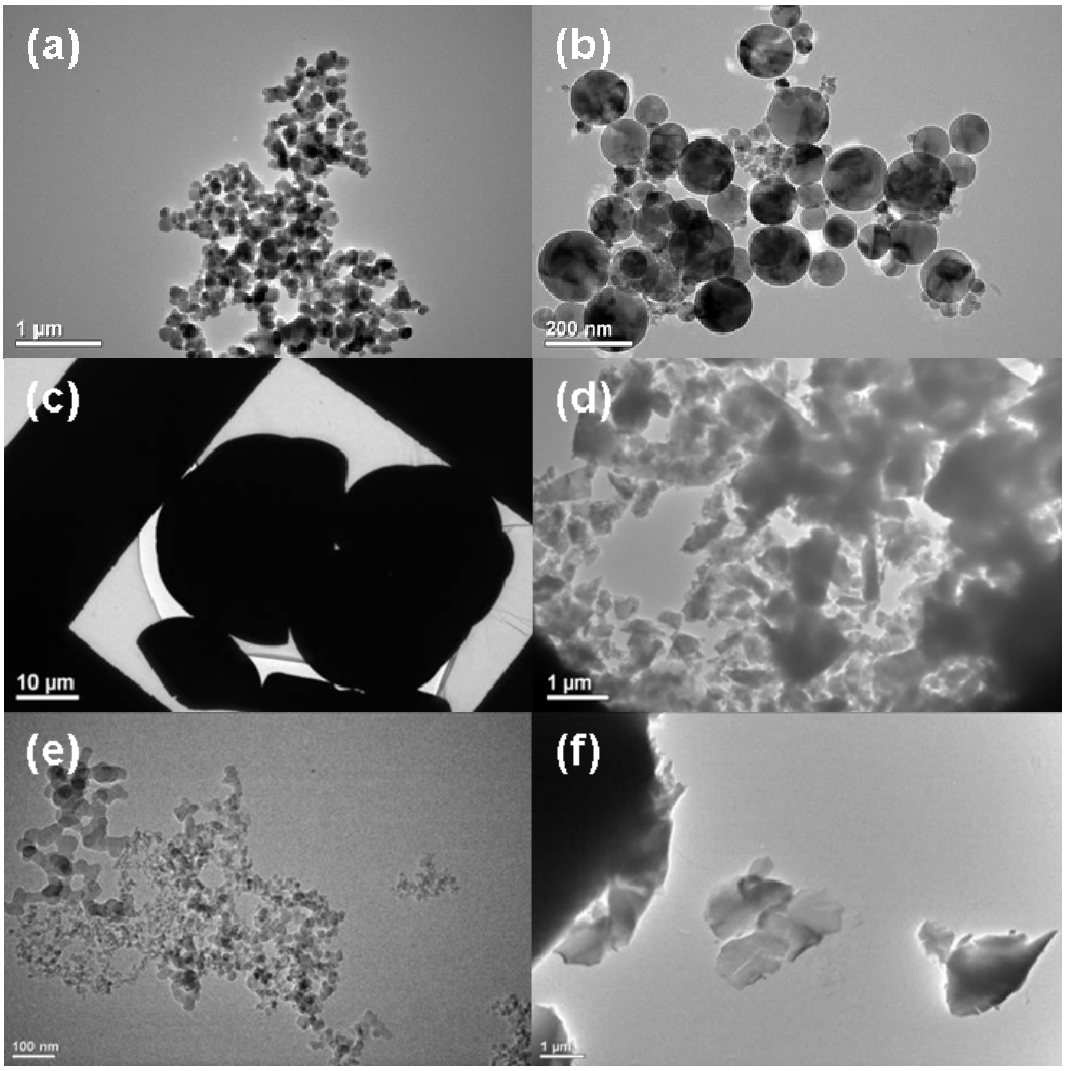

Fig. 8. Representative TEM images of metal oxides. (a) Commercial Anatase TiO_2 (Ti-A), (b) Synthesized Anatase TiO_2 (Ti-S), (c) Commercial Rutile TiO_2 (Ti-R), (d) MIN-U-SIL 5 Crystalline silica (Si-C), (e) CAB-O-SIL M-5 Amorphous silica (Si-A), (f) Silicon(IV) oxide (Si-S).

Standard Reference Materials (SRMs)

The standard reference materials; diesel particulate matter (DPM) and urban particulate matter (UPM) were purchased from National Institute of Standard and Technology (NIST, Gaithersburg, MA). The detailed information is provided in Table 5, and the results of TEM and EDS analysis are shown in Fig. 9.

Table 5. Sample information of standard reference materials.

Sample ID	Materials	Characteristics	Id # CAS/Lot	Supplier
DPM	Diesel Particulate Matter	Diameter : 5 - 30 nm	2975	NIST
UPM	Urban Particulate Matter	200 nm – 100 μm (mode : 20 μm)	1648a	

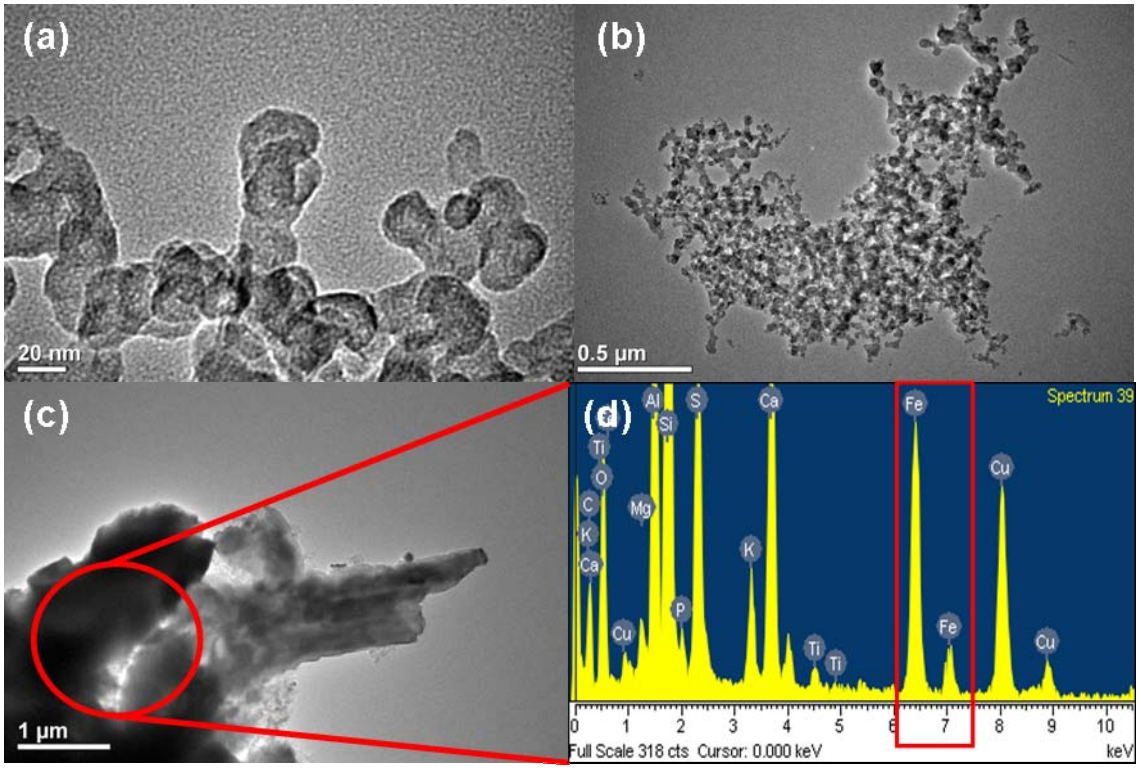

Fig. 9. TEM and EDS results of SRMs. (a) and (b) Representative TEM images of DPM, (c) Representative TEM image of UPM, (d) EDS results of UPM, the red circle indicate the spot where EDS analysis was done.

The EDS result confirms UPM particles have a considerable amount of Fe which may interfere the reductive capacity assay.

4.2 Carbon Nanomaterials

Carbon Nanotubes (CNTs)

The reductive capacity of different types of pristine and modified CNTs was measured using aforementioned method, and the results are within range of 1.1×10^{-3} ~ 8.4×10^{-3} g/g as shown in Fig. 10.

In general, single-wall carbon nanotubes (SCNTs) appeared to have higher reductive capacity than multi-wall carbon nanotubes (MCNTs) which is most likely due to higher specific surface area (SSA, m^2/g) shown in Table 6. The results of SCNTs with functional groups show that hydroxyl (OH) surface groups help reduction of Fe^{3+} through the following reaction:

$$\sim C\text{-}OH + Fe^{3+} \rightarrow \sim C = O + Fe^{2+} + H^{+} \text{ [48].}$$

The reductive capacity of SCNT with carboxyl (COOH) surface functional groups appeared to be 9.3 % lower than that of pristine SCNT, however, the difference is not significant based on the t-test. According to the ANOVA test, the differences of mean of reductive capacities both within SCNTs and within MCNTs are significant but not within the group of MCNTs when MCNT_2 was excluded.

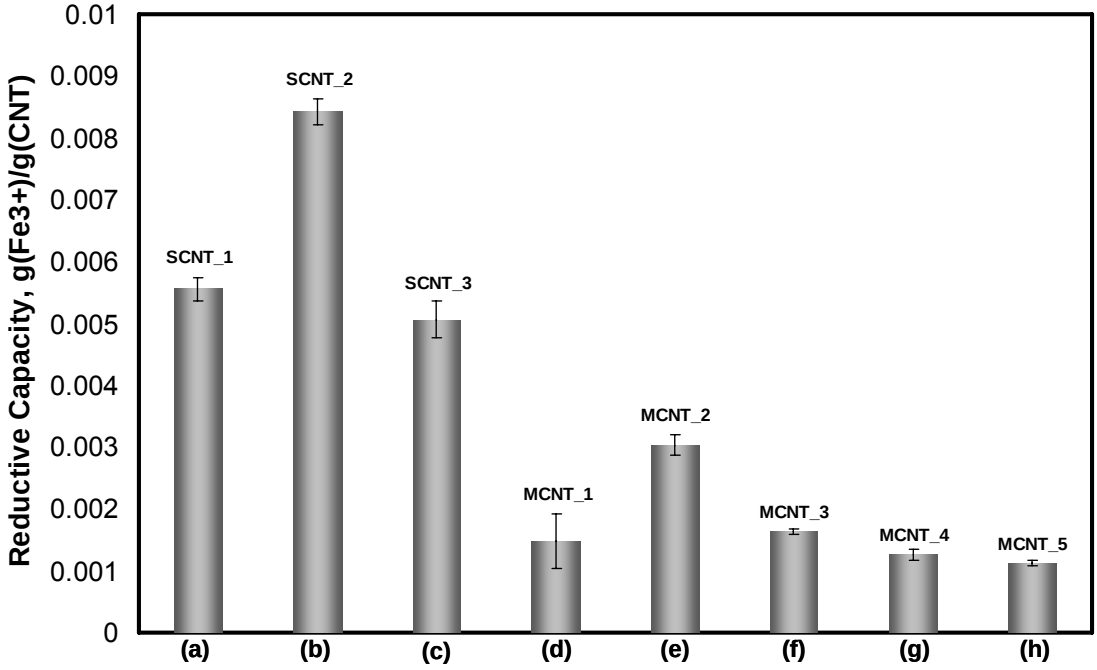

Fig. 10. Reductive capacity of CNTs. (a) Pristine single-wall CNT, (b) Single-wall CNT with OH groups, (c) Single-wall CNT with COOH groups, (d) Multi-wall CNT with outer diameter (OD) of < 8 nm, (e) Multi-wall CNT with OD of 10 - 20 nm, (f) Multi-wall CNT with OD of > 50 nm, (g) Graphitized MCNT_2, (h) Graphitized MCNT_3.

Table 6. Specific surface area (SSA) and reductive capacity of CNTs in surface area basis.

	SSA[a] (m^2/g)	Reductive Capacity (g/g)	Reductive Capacity (g/m^2)
SCNT_1	425	$5.56\times10^{-3} \pm 1.87\times10^{-4}$	$1.31\times10^{-5} \pm 4.39\times10^{-7}$
SCNT_2	336	$8.42\times10^{-3} \pm 2.09\times10^{-4}$	$2.51\times10^{-5} \pm 6.21\times10^{-7}$
MCNT_2	154	$3.03\times10^{-3} \pm 1.68\times10^{-4}$	$1.97\times10^{-5} \pm 1.09\times10^{-6}$
Ground MCNT_2	168	$4.52\times10^{-3} \pm 1.58\times10^{-4}$	$2.69\times10^{-5} \pm 9.4\times10^{-7}$

[a]SSA of CNTs was determined by BET measurements.

The graphitized forms (MCNT_4 and MCNT_5) showed significantly lower reductive capacity than that of pristine forms (MCNT_2 and MCNT_3) as summarized in Table 7, and the graphitization was confirmed by Raman spectra as seen in Fig. 11.

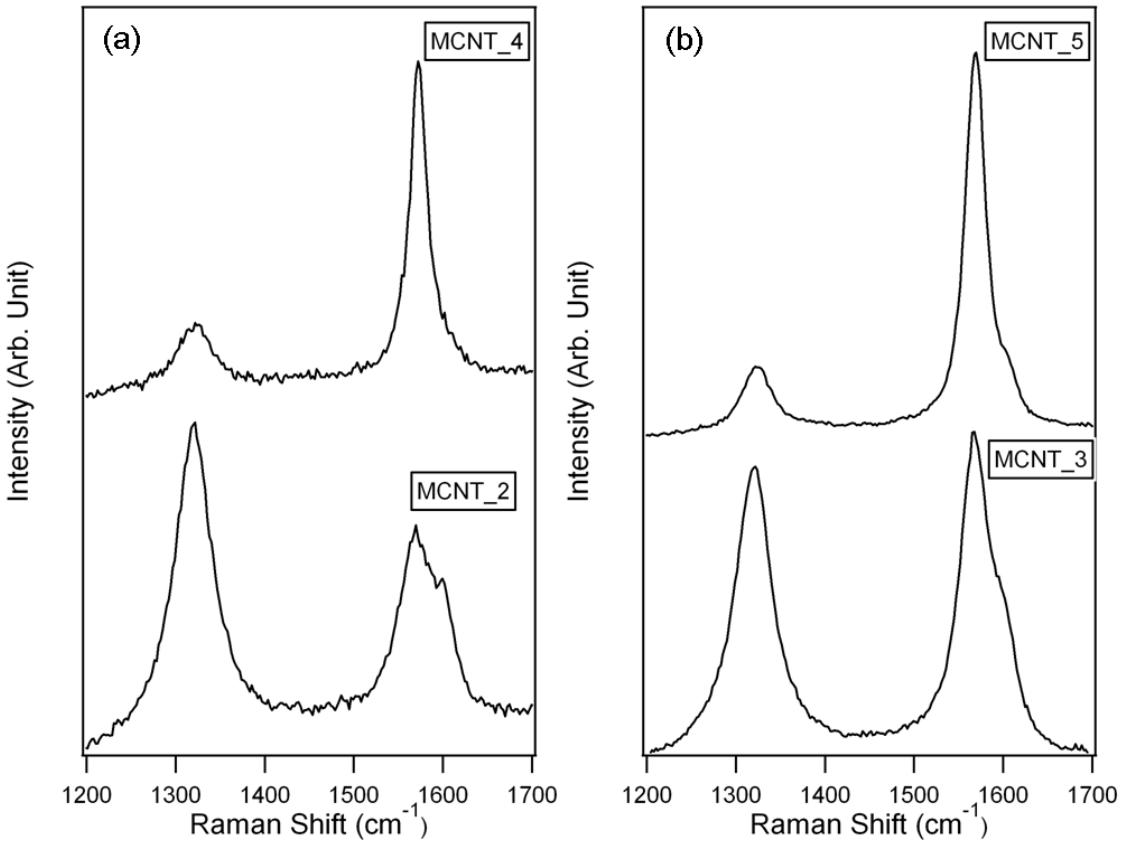

Fig. 11. Raman spectra of (a) MCNT_2 and MCNT_4, (b) MCNT_3 and MCNT_5. Two main peaks appeared at 1320 cm^{-1} and 1570 cm^{-1}; the peak at 1320 cm^{-1} is associated with structural defect (D band), while the peak at 1570 cm^{-1} corresponds to carbon-carbon bonding in a graphene sheet (G band).

The intensity ratio of $I_G/(I_D + I_G)$, where I_D and I_G is the intensity of D band at 1320 cm^{-1} and G band at 1570 cm^{-1}, respectively, indicates the degree of graphitization of CNTs, and the ratio increases as a CNT is graphitized [49].

Table 7. Degree of graphitization and reductive capacity of MCNTs.

Material	Degree of graphitization[a]	Increase	Reductive Capacity	Decrease
MCNT_2	0.4484	46.2 %	3.027×10^{-3}	58.4 %
MCNT_4	0.6558		1.261×10^{-3}	
MCNT_3	0.5201	47.2 %	1.642×10^{-3}	31.3 %
MCNT_5	0.7653		1.128×10^{-3}	

[a] Degree of graphitization is the ratio of $I_G/(I_D + I_G)$.

The decreased reductive capacity of graphitized CNTs can be explained by the fact that the graphitization process results in decrease of both surface area and structural defects.

As seen in Fig. 12, it was found that reductive capacity of CNTs could be significantly increased by 30~50 % after the grinding, and 3 days of aging could make them lose some of enhanced reductive capacity. Structural defects, confirmed by TEM images of ground MCNT_3 in Fig. 6 and Raman spectroscopy in Fig. 13, were generated by grinding using a mortar and pestle for 20 minutes by hand. The increased reductive capacity should be explained by the fact that grinding CNTs results in not only increase of specific surface area but also generation of reactive sites following rupture of carbon-carbon covalent bonding [50]. Since the active sites on the defects by grinding are easily

oxygenated by ambient air [50], the grinding-induced reactive sites lose their ability to reduce Fe^{3+} ions after sufficient period of time passed.

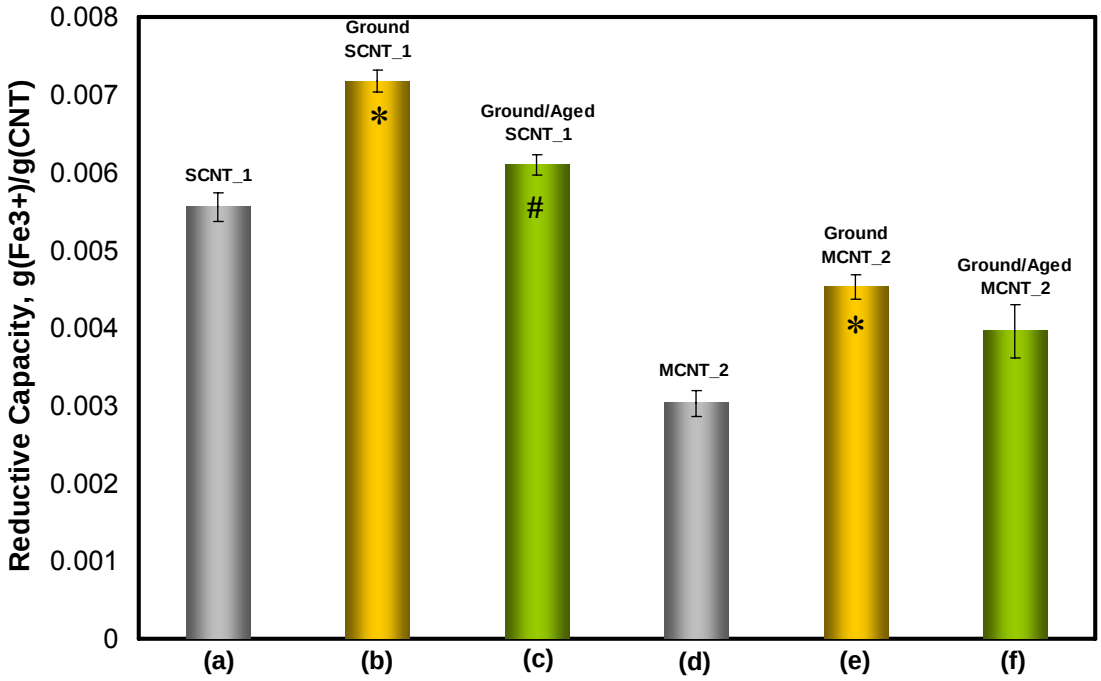

Fig. 12. Reductive capacity of modified CNTs by grinding and aging. (a) Pristine SCNT_1, (b) Ground SCNT_1, (c) Ground and aged SCNT_1, (d) Pristine MCNT_2, (e) Ground MCNT_2, (f) Ground and aged MCNT_2.

'*' means significantly different from the corresponding pristine sample.

'#' indicates reductive capacity of the aged sample is significantly different from ground sample.

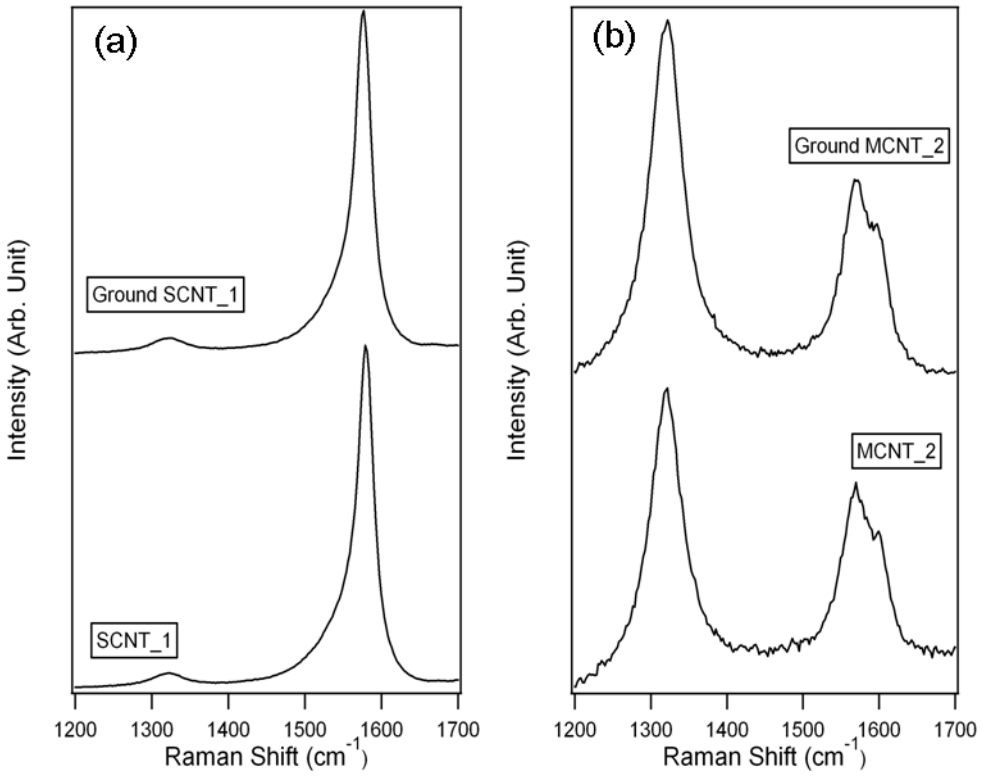

Fig. 13. Raman spectra of pristine and ground CNTs. (a) SCNT_1 and ground SCNT_1, (b) MCNT_2 and ground MCNT_2.

The ratio of I_D and I_G can be also used to determine the extent of defects in CNTs [51], and the values of I_D / I_G are reported in Table 8.

Table 8. The extent of defects on CNTs, I_D / I_G.

Material	Pristine form	Ground form	Increase
SCNT_1	0.0729	0.0739	1.37 %
MCNT_2	1.23	1.46	18.77%

The ratio, I_D / I_G, increased in both cases upon grinding, confirming that structural defects were generated by grinding. And grinding turned out to be more effective on MCNTs than SCNTs in terms of generating of defects, because MCNTs can have more active sites on its cross section when they are cut and broken by grinding.

Sonication prior to the incubation increased only reductive capacity of SCNT_1 by 17 % while its application did not cause any significant differences on other CNTs including SCNT_2, SCNT_3 and MCNT_2 as shown in Fig. 14.

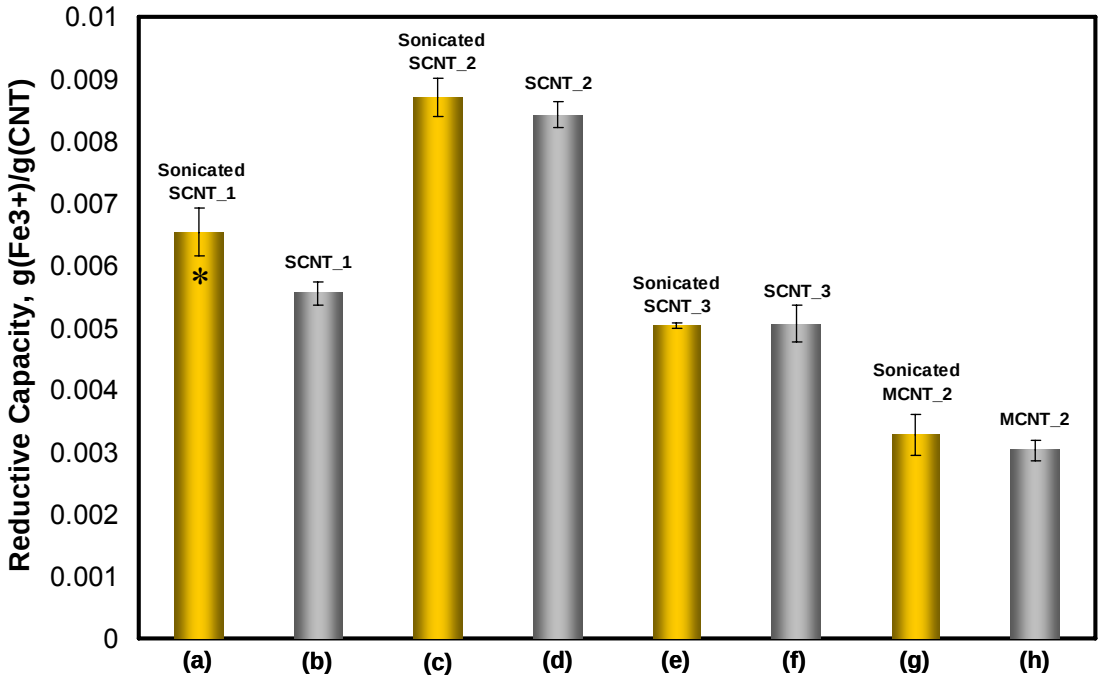

Fig. 14. Effect of sonication on reductive capacity of CNTs.
'*' means significantly different from pristine sample.

Carbon Black (CB) and Acetylene Soot (Soot-A)

The pristine form of CB and Soot-A were tested for the reductive capacity, and both materials were oxidized as described in appendix A and used for the reductive capacity analysis. The results in Fig. 15 show CB has the highest reductive capacity (9.3×10^{-3} g/g) among examined materials in this study, and it lost 34 % of the reduction ability after oxidization. Soot-A had reductive capacity of 3.4×10^{-3} g/g and 2.3×10^{-3} g/g before and after oxidization, respectively. The results show that 2 weeks of oxidization weakened the reduction ability of both carbon materials by almost 1/3.

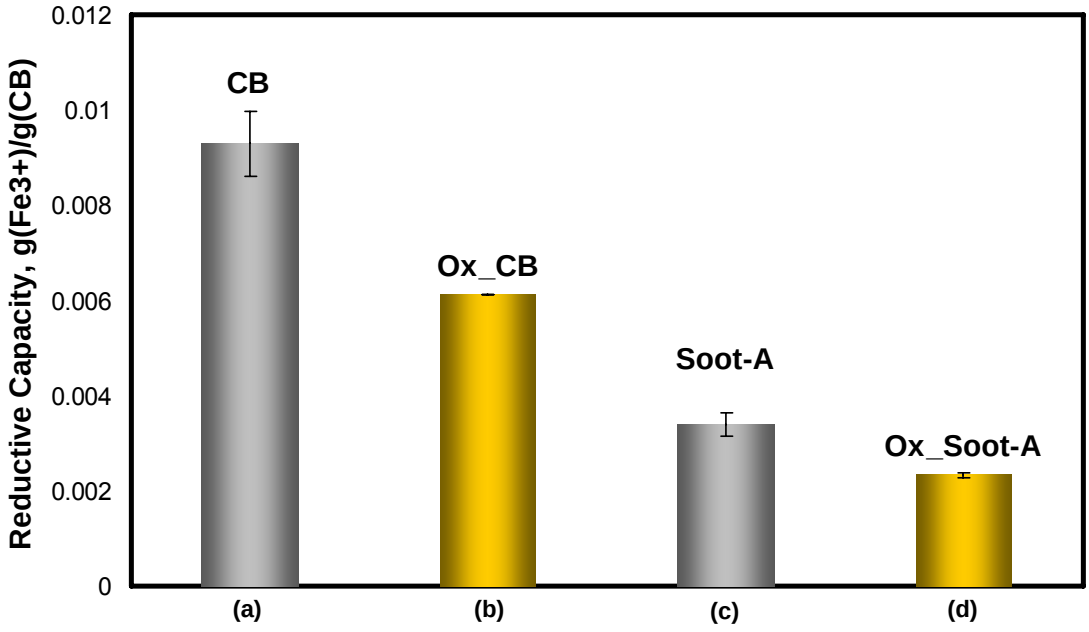

Fig. 15. Reductive capacity of CB and Soot. (a) Pristine CB, (b) Oxidized CB, (c) Pristine Soot-A, (d) Oxidized Soot-A.

Fullerenes (C_{60})

Fullerenes (C_{60}) exhibited different reductive capacities, depending on the its surface functional groups; C_{60} with OH groups turned out to be strongly reductive towards Fe^{3+}, and C_{60} with H atoms on its surface has moderate reductive capacity while pristine C_{60} is not able to reduce significant amount of Fe^{3+} as shown in Fig. 16. Effect of OH groups was explained with CNTs above, and H atoms on the surface also can be involved in redox reactions as shown below:

$$\sim C\text{-}H + Fe^{3+} + H_2O \rightarrow \sim C\text{-}OH + Fe^{2+} + H^+$$

$$\sim C\text{-}H + Fe^{3+} + H_2O \rightarrow \sim C{=}O + Fe^{2+} + H^+ \text{ [48].}$$

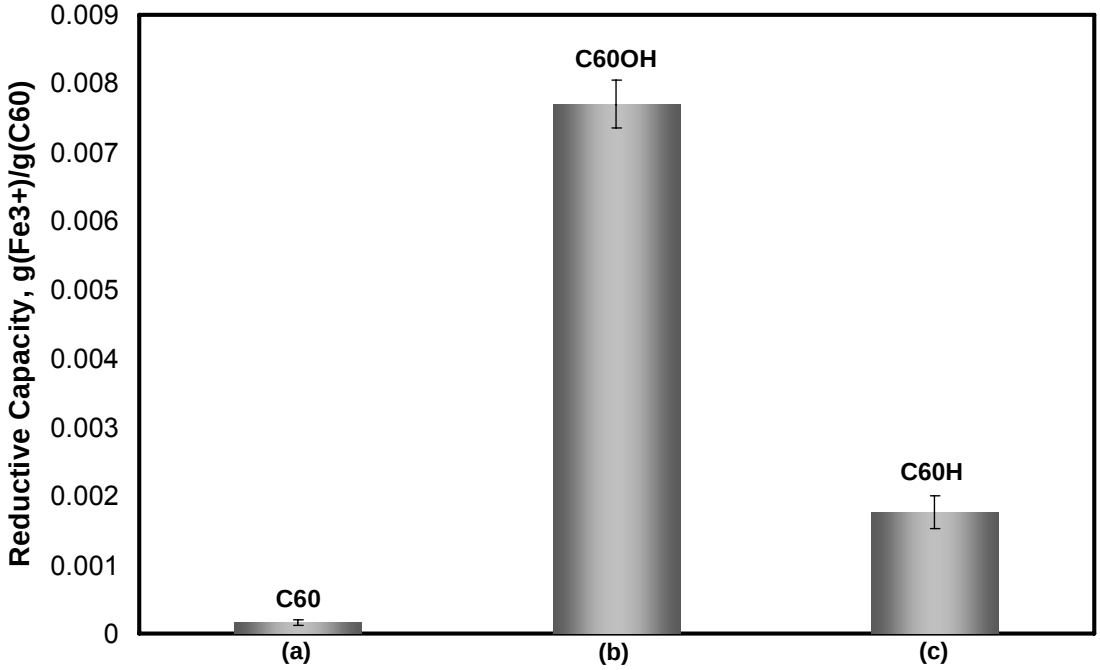

Fig. 16. Reductive capacity of fullerenes. (a) Pristine C_{60}, (b) C_{60} with OH groups, (c) C_{60} with H atoms.

4.3 Metal Oxides

Titanium Dioxides (TiO_2)

The reductive capacity of three different TiO_2 was investigated; commercial anatase TiO_2 (Ti-A), synthesized anatase TiO_2 (Ti-S) and commercial rutile TiO_2 (Ti-R). Even though Ti-A has the highest reductive capacity among tested TiO_2, reductive capacities of TiO_2 are relatively low compared to that of CB which means the differences within TiO_2 may not be significant in terms of biological effects. In Fig. 17, the results of TiO_2 are shown in comparison with that of CB.

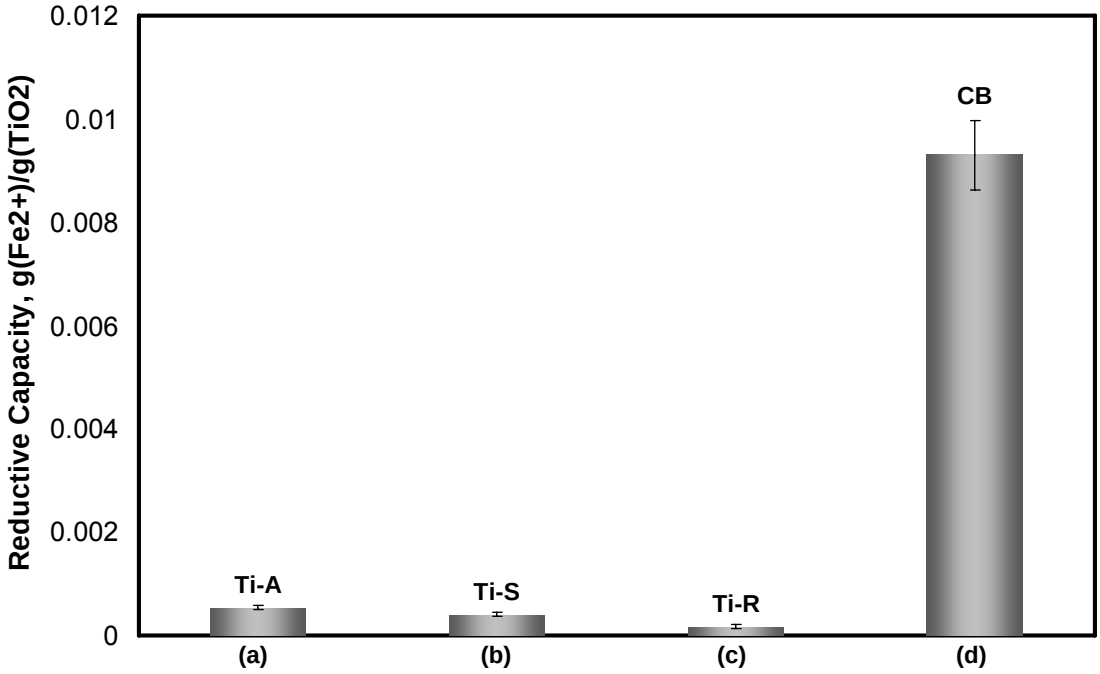

Fig. 17. Reductive capacity of TiO_2 in comparison with CB. (a) Commercial anatase TiO_2 (b) Lab synthesized TiO_2 (c) Commercial rutile TiO_2 (d) CB.

Silicon Dioxide (SiO_2)

Various types of silica were examined and resulted in no significant reductive capacity from all three different types of silica. Reductive capacities of silica are within range of $8.8\times10^{-5} \sim 1.3\times10^{-4}$ g/g which is within measurement uncertainty (1.4×10^{-4} g/g) due to the limit of the spectrophotometer sensitivity (0.002 in absorbance). The reductive capacity of silica is summarized in Fig. 18. The conversion of absorbance limit to measurement uncertainty is shown in appendix D.

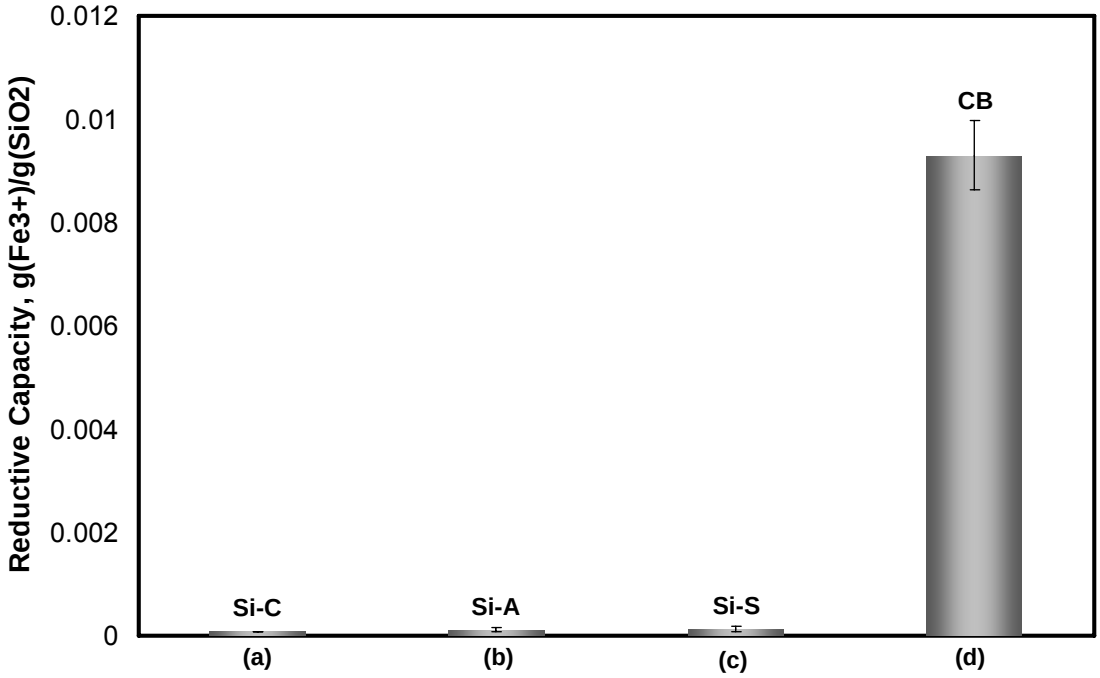

Fig. 18. Reductive capacity of silica. (a) MIN-U-SIL 5 Crystalline silica, (b) CAB-O-SIL amorphous silica, (c) Silicon(IV) oxide, (d) CB.

4.4 Standard Reference Materials (SRMs)

The diesel particulate matter (DPM) and urban particulate matter (UPM) from NIST were analyzed, and the results, shown in Fig. 19, indicate that both particulate matters have considerable reductive capacity of 2.5×10^{-3} g/g. As seen in EDS result in Fig. 9, UPM contains a significant amount of Fe in it, and extractable Fe^{2+} was determined as 1.4×10^{-3} g/g at the same condition with the standard method described in appendix C. The reductive capacity of UPM was obtained after subtracting extractable Fe^{2+}.

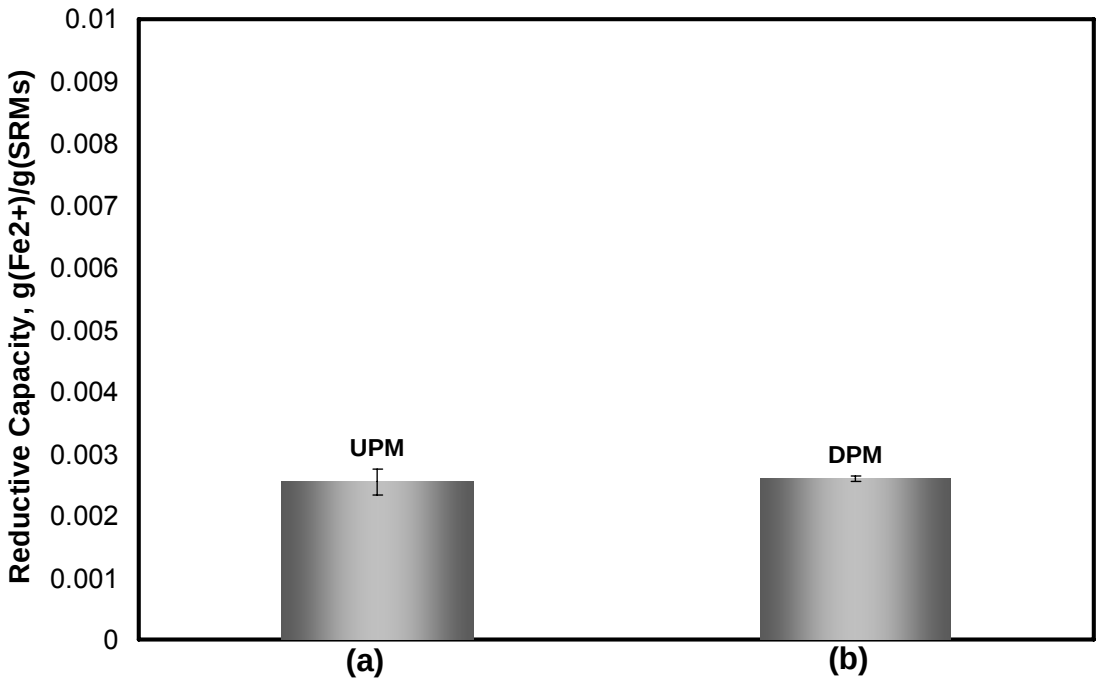

Fig. 19. Reductive capacity of SRMs. (a) Urban particulate matter, (b) Diesel particulate matter.

5. STANDARDIZATION OF THE METHOD

Each step of spectrophotometric method may be affected by various factors, resulting in significant errors. These factors needed to be investigated and corrected so that we could get a consistent and compatible reductive capacity results. By eliminating unnecessary factors and minimizing variables, a reproducible method was established. Besides, due to the differences in the nature of the materials, additional steps were required in case of hydrophobic or unfiltered particles. And the addition of selective steps enabled this method to be applied for various types of nanomaterials without distortion of the results.

5.1 Preparation of Incubation Solutions

Fe Salt Selection

Iron(III) sulfate hydrate ($Fe_2(SO_4)_3 \cdot xH_2O$, Reagent grade, Alfa Aesar, Ward Hill, MA), iron(III) chloride hexahydrate ($FeCl_3 \cdot 6H_2O$, ACS, Alfa Aesar, Ward Hill, MA), iron(III) nitrate nonahydrate ($Fe(NO_3)_3 \cdot 9H_2O$, > 98 %, Alfa Aesar, Ward Hill, MA) and iron(III) oxide (Fe_2O_3, maghemite, Labaratory generated [25]) were tested to be used for the initial ferric aqueous solution by criteria of ease of use and stable color development.

Fe_2O_3 was once used to measure the reductive capacity of carbon black in 0.75M sulfuric acid [41], and this concentration of sulfuric acid gives too low pH (-0.18) which

is not possible in human cell culture [52]. To see if Fe_2O_3 nanoparticles are soluble in bioavailable pH (>3.5), 20mg of Fe_2O_3 particles were incubated at different pH for 16 hours. The quantities of Fe_2O_3 nanoparticles and sulfuric acid used in each case are shown in Table 9.

Table 9. The quantities of Fe_2O_3 nanoparticles and sulfuric acid.

Fe_2O_3	Sulfuric Acid (concentration)	DI water	pH in the solution
20 mg	0.02 ml (5%)	75 ml	3.41
20.2 mg	0.5 ml (20%)		1.71
21.1 mg	1 ml (20%)		1.4

The leached Fe^{2+} and Fe^{3+} from Fe_2O_3 at each pH were determined using spectrophotometric method, and the results are shown in terms of weigh percentage (Leached Fe / Used Fe_2O_3 ×100) in Fig. 20.

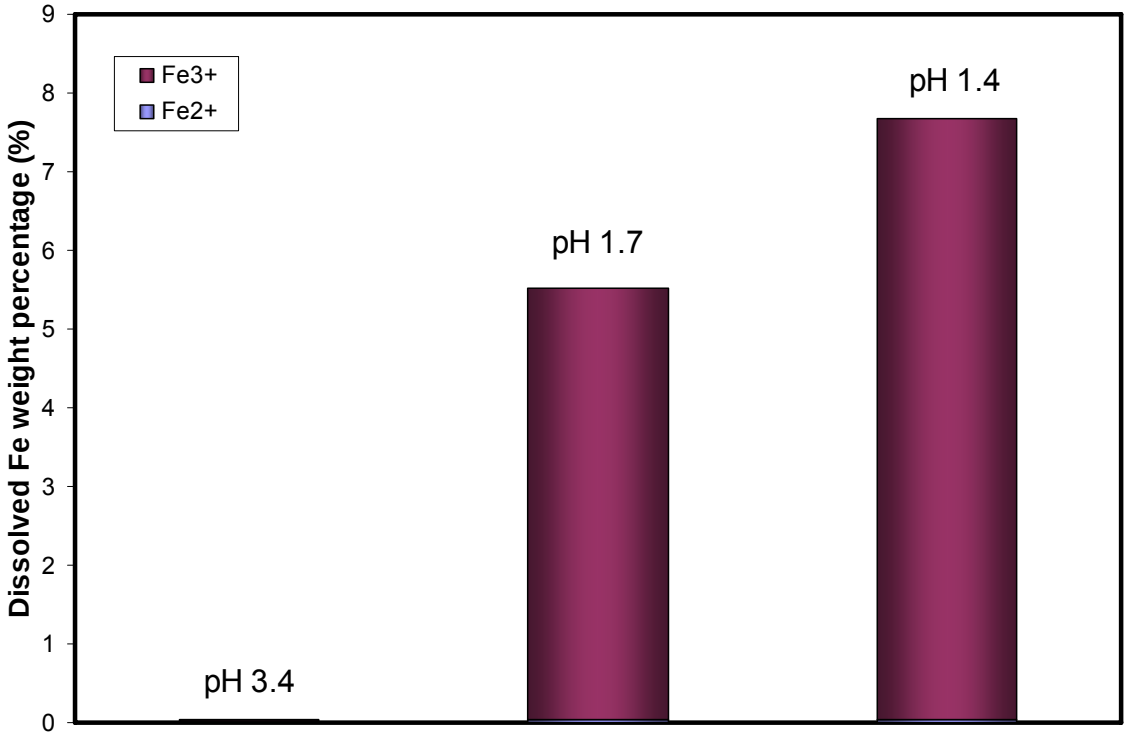

Fig. 20. Leached Fe ions from Fe_2O_3 in the solutions of different pH. The amount of Fe^{2+} leached from Fe_2O_3 is below the measurement uncertainty regardless of pH.

The results show that while considerable amount of Fe was dissolved at pH 1.7 and 1.4, there was almost no leachable Fe ions at the pH 3.4. This suggests that we have to use pH lower than bioavailable limit to prepare ferric solution with Fe_2O_3, and the applications of this method using Fe_2O_3 are likely to be limited to only a few cases allowing strong acidic condition.

Iron chloride ($FeCl_3$) was also considered as a candidate for trivalent Fe salt, but it was removed from the list of candidates due to its time consuming color development. A stock solution of $FeCl_3$ was prepared with 46mg of iron(III) chloride hydrate in 1 L of DI water, and 50ml of the stock solution and reagents were added into each flask as

summarized in Table 10. 5 % sodium acetate anhydrous (CH_3COONa, 99 %, Alfa Aesar) and 20 % sulfuric acid (H_2SO_4, 95%, Labchem, Pittsburgh, PA) were used to adjust pH in the solutions for absorbance reading. The absorbance of each solution of flask was measured by spectrophotometer at various time lapsed from 10 to 1380 minutes.

Table 10. Chemicals added into each flask for $FeCl_3$ color development.

Flask No. / pH	(1)/1.47	(2)/1.94	(3)/5.76	(4)/6.42	(5)/6.95	(6)/7.17
Stock solution	50ml	50ml	50ml	50ml	50ml	50ml
1% Hydroquinone	1ml	1ml	1ml	1ml	1ml	1ml
20% sulfuric acid	1ml	0.25ml	•	•	•	•
5% Sodium acetate	•	•	•	1ml	5ml	10ml
0.3% Phenanthroline	10ml	10ml	10ml	10ml	10ml	10ml

Color developments of $FeCl_3$ with phenanthroline at different pH are plotted in Fig. 21.

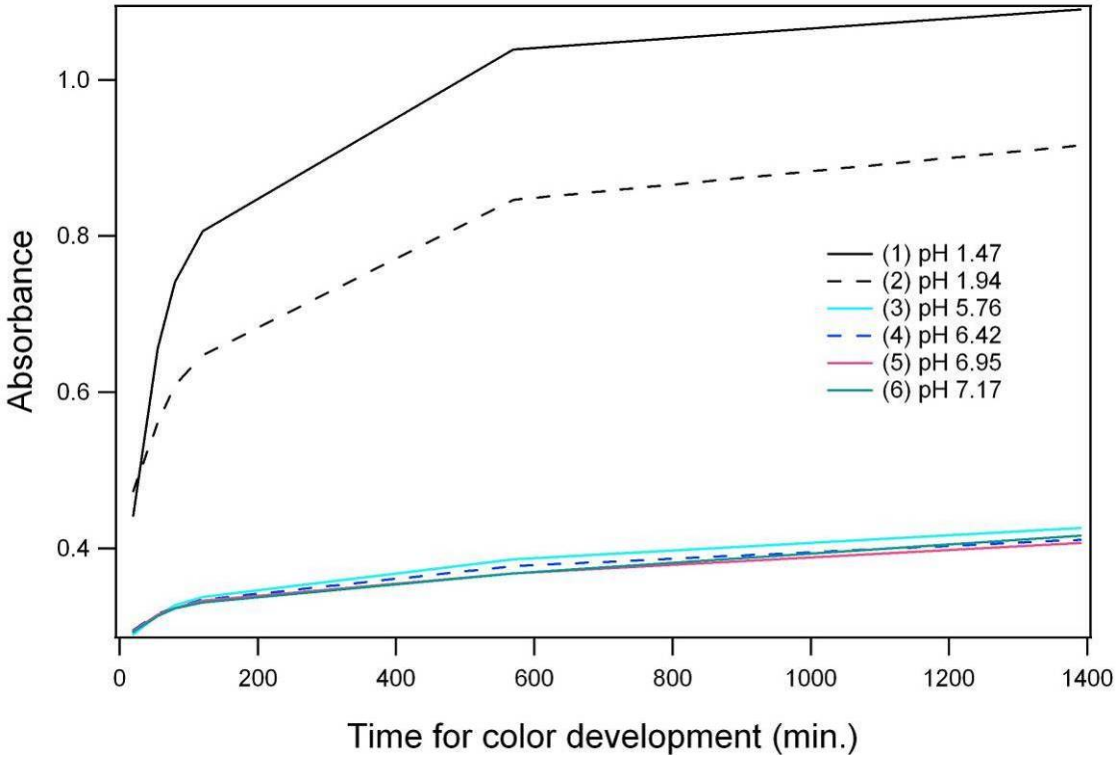

Fig. 21 Color development of $FeCl_3$ solution at different pH at Fe concentration of 4.75mg/L.

The graphs in Fig. 21 show that lower pH is favorable condition for higher absorbance. However, the color of $FeCl_3$ solutions were not completed and steady even after 10 hours of color development, and it seems that using $FeCl_3$ makes the procedure less efficient due to the sluggish color development.

Iron nitrate ($Fe(NO_3)_3$) was ruled out from the list of the Fe salts due to the its highly hygroscopic property. To obtain accurate calibration curve, it is necessary to know the exact amount of Fe used within error of ± 0.2 mg. During weighing $Fe(NO_3)_3$ on the scale, the actual mass kept increasing due to the adsorption of moisture in ambient

air, and it was inevitable to lose some of weighed iron nitrate because they were molten and stuck on the weighing paper.

Satisfying ease of use and stable and quick color development, Iron sulfate ($Fe_2(SO_4)_3$) was selected to be used for ferric solution for the reductive capacity assay. For the stock $Fe_2(SO_4)_3$ solution, 50.7 mg of Iron(III) sulfate hydrate ($Fe_2(SO_4)_3 \cdot xH_2O$, Reagent grade) was dissolved in 1 L of DI water. 50 ml of the stock solution and 1 ml of 1 % hydroquinone were put into five 100 ml volumetric flasks, and different amounts of 20 % sulfuric acid or 5 % sodium acetate were added to get various pH. And then, 10 ml of 0.3 % phenanthroline was added into all flasks. A method blank solution which contained only 50 ml of the stock solution and hydroquinone was made to see the background absorbance of the solutions. All of six flasks were diluted to 100 ml and measured its absorbance at different times ranging from 5 to 210 minutes. The quantities of chemicals which each flask contained are shown in Table 11.

Table 11. Chemicals added into each flask for $Fe_2(SO_4)_3$ color development.

Flask No./pH	(1)/1.9	(2)/2.48	(3)/5.9	(4)/6.9	(5)/7.21	(6)
Stock solution	50ml	50ml	50ml	50ml	50ml	50ml
1% Hydroquinone	1ml	1ml	1ml	1ml	1ml	1ml
20% sulfuric acid	0.25ml	0.1ml	•	•	•	•
5% Sodium acetate	•	•	•	2ml	10ml	•
0.3% Phenanthroline	10ml	10ml	10ml	10ml	10ml	•

The measured pH of each solution was 1.9, 2.48, 5.9, 6.9, 7.21, respectively. The absorbance results are plotted in Fig. 22.

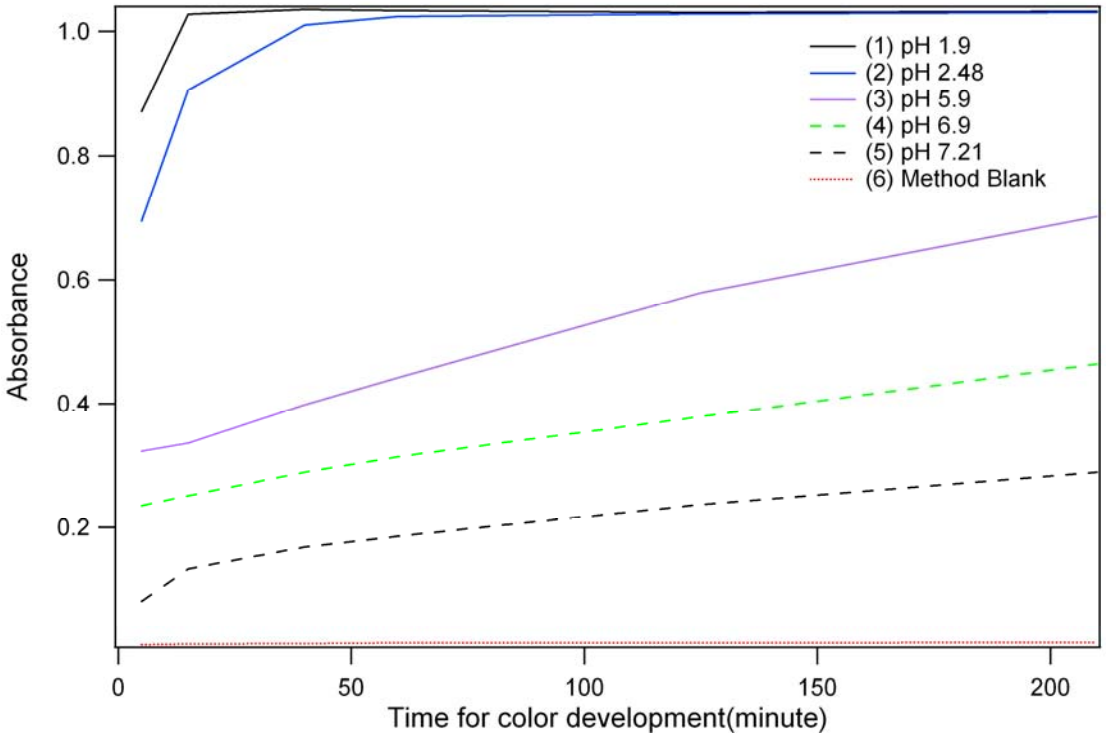

Fig. 22. Color development of $Fe_2(SO_4)_3$ solution at different pH at Fe concentration of 5.56 mg/L.

Color development of $Fe_2(SO_4)_3$ solution with phenanthroline is certainly pH dependant, and the curves show that the lower pH of the solution is favorable for quick color development. In case of pH 1.9, it completed color development within 30 minutes and went steady which makes it desirable to use pH 2 for absorbance measurement.

Effect of Fe Ratio to Nanomaterials in the Incubation Solution

Effect of Fe ratio on reductive capacity of CB was investigated by either varying usage of $Fe_2(SO_4)_3$ with fixed amount of CB at 30 mg or varying amount of CB with

fixed $Fe_2(SO_4)_3$ usage at 9 mg. And the reductive capacity results measured from different Fe ratio were compared with redox capacity result measured by the standard method (30mg of CB and 9mg of $Fe_2(SO_4)_3$). When the amount of $Fe_2(SO_4)_3$ was varied, controls having the same amount of $Fe_2(SO_4)_3$ were used to see if Fe^{3+} ions are able to be reduced without any reducing agent at high concentration, and the absorbance of each control was measured with the same method as used for the reductive capacity measurement. Each reductive capacity was obtained from triplicate measurements, and the quantities of CB and $Fe_2(SO_4)_3$ in incubation solutions were shown in Table 12.

Table 12. The quantities of CB and Fe in the incubation solutions.

Sample No.	CB	$Fe_2(SO_4)_3$	Fe ratio to CB (g/g)	DI water
1-1	30 ± 0.4 mg	3 ± 0.3 mg	0.022	75 ml
1-2	30 ± 0.4 mg	30 ± 0.8 mg	0.216	
1-3	30 ± 0.4 mg	90 ± 1.1 mg	0.658	
2-1	90 ± 0.6 mg	9 ± 0.4 mg	0.022	
2-2	10 ± 0.2 mg	9 ± 0.2 mg	0.197	
Standard	30 ± 0.2 mg	9 ± 0.2 mg	0.066	
Controls	.	2.8 mg	.	
		8.9 mg		
		30.1 mg		
		89.4 mg		

Dissolved $Fe_2(SO_4)_3$ can react with phenanthroline, resulted in yellow color which can be attributed to binuclear complexes [53]. And the absorbance results in Fig. 23 show that the interference due to reaction between Fe^{3+} and phenanthroline becomes more significant at higher Fe^{3+} concentration. Since the ferroin has red color, the yellow color of the solution, shown in Fig. 24, indicates the color was not caused by Fe^{2+}.

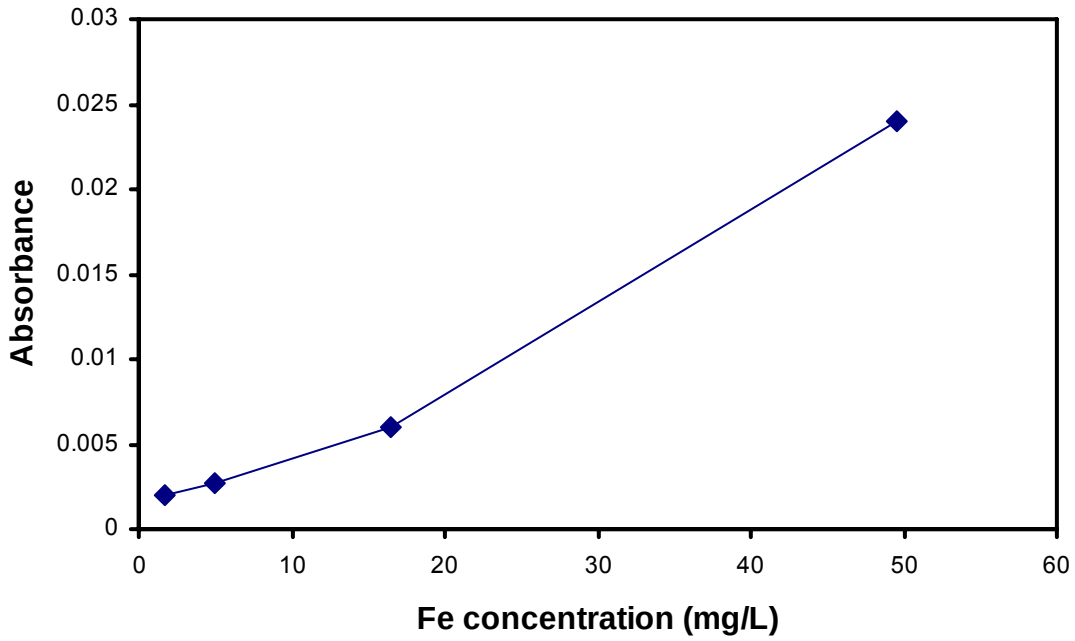

Fig. 23. Color intensity of $Fe_2(SO_4)_3$ control solutions.
*Absorbance was read with solutions containing 25 ml of incubated solution, 0.25 ml of 20% sulfuric acid, 10 ml of 0.3% phenanthroline out of 100 ml at 512 nm.

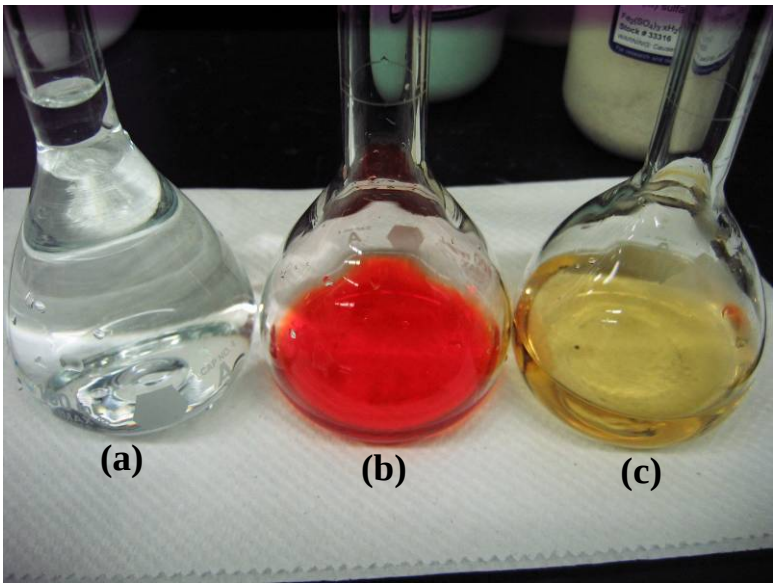

Fig. 24. A photo of 90 mg of $Fe_2(SO_4)_3$ control. (a) Method blank, (b) Fe total, (c) Fe^{2+}.

The absorbance results from controls were taken into account for calculating reductive capacity of each sample, and the results were summarized in Table 13 and Fig. 25.

Table 13. Fe ratio and reductive capacity of each sample.

Sample No.	Fe ratio to CB (g/g)	Reductive Capacity (g/g)
1-1	0.022	0.0042
1-2	0.216	0.0151
1-3	0.658	0.0215
2-1	0.197	0.0121
2-2	0.022	0.0066
Standard	0.066	0.0093

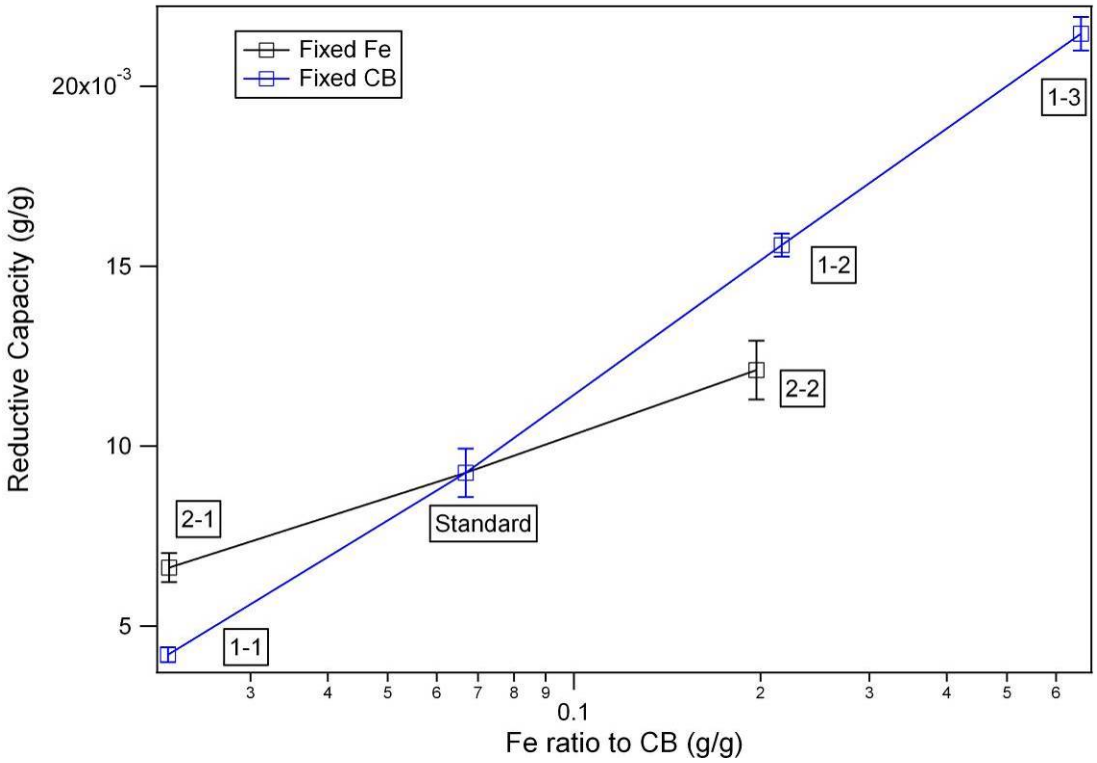

Fig. 25. Effect of Fe ratio on the reductive capacity of CB.

The results clearly show that reductive capacity is function of Fe ratio, and thus it was concluded that we should use constant Fe ratio to generate comparable results.

Mixing Nanomaterials

Since the reduction of Fe^{3+} ions by nanomaterials occurrs in an aqueous solution, all the nanomaterials need to be submerged in the solution. To avoid floating of hydrophobic particles such as C_{60} and graphitized CNTs, different types of additives including alcohols and surfactant were tried to make the hydrophobic particles wet. All

of these additives were able to wet hydrophobic particles, and effects of adding alcohols and surfactant on the reductive capacity was investigated using CB. Each type of alcohols or diluted surfactant Tween 20 solutions (0.12 mM) was added first to soak CB and $Fe_2(SO_4)_3$, and the reductive capacity assay was then carried out. The quantities of additives in the incubation solutions are shown in Table 14.

Table 14. The quantities of additives in the incubation solutions

Sample ID.	Quantity	Additive
Control	·	·
Isopropanol	0.5 ml	Isopropyl Alcohol (>99.5%, Mallinckrodt)
Aceton	0.5 ml	Aceton (>99.5%, Sigma-Aldrich)
Butanol	2 ml	Butyl Alcohol (>99.4%, Mallinckrodt)
Surfactant	2 ml (0.12mM)	Tween 20 (Bio Rad)

Fig. 26 shows surfactant makes hydrophobic C_{60} get submerged into water.

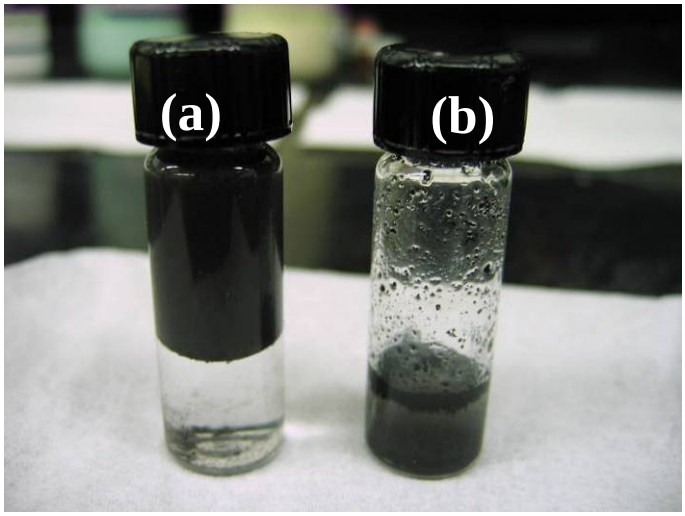

Fig. 26. A photo showing of the behavior of a hydrophobic material; 30 mg of C_{60} in (a) DI water and (b) 0.12mM surfactant solution.

The reductive capacity results of CB with different additives were summarized in Fig. 27.

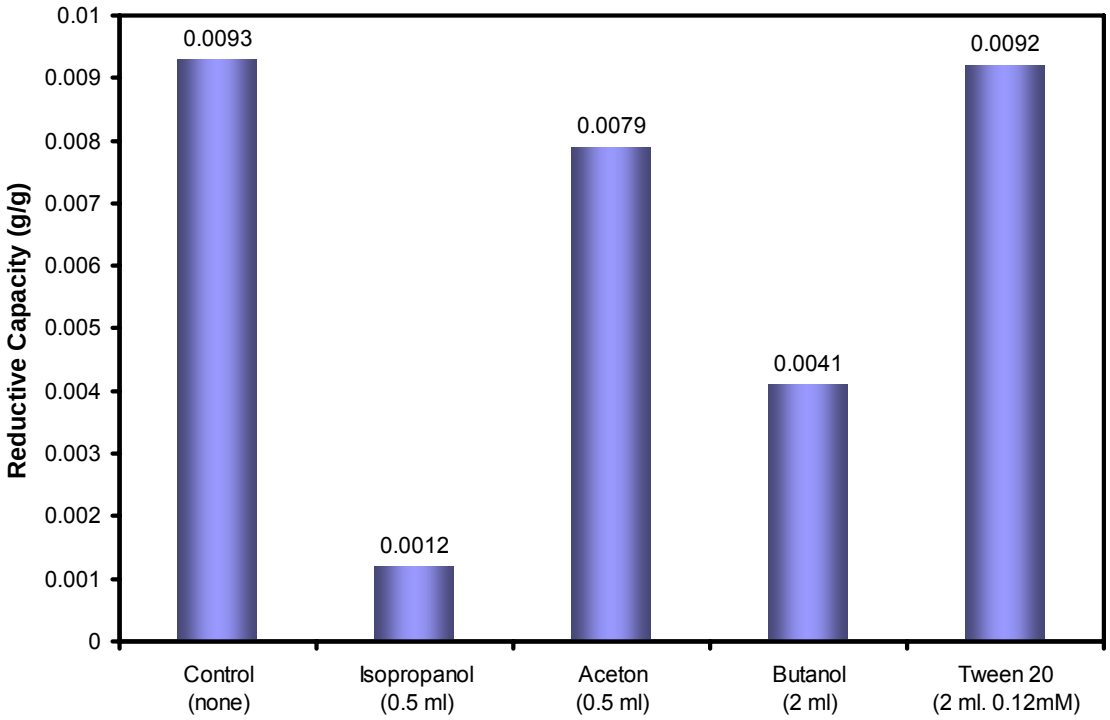

Fig. 27. Effect of surfactants on the reductive capacity of CB.

The results show that all alcohols interfere with the reductive capacity measurement, resulting in decreased reductive capacity while surfactant could be employed without significant interferences.

Sonication was once considered as a way to help dispersion of nanomaterials in solutions, and it might also help increase actual surface area, leading increased reductive capacity as seen in Fig. 14. However, it is decided not to use sonication not only because it is not likely to happen in biological conditions but also because it could influence incubation solution chemically which may affect the reductive capacity [54].

5.2 Incubation

Temperature

The incubation temperature was set to 37 ˚C to mimic human cell culture.

Incubation Time

In order to assure the reduction reaction of nanomaterials is fully completed, it was required to give nanomaterials sufficient incubation time to react with Fe^{3+} in the solutions. To determine effect of incubation time, a time course of the reductive capacity was obtained with CB by varying incubation time from 1 to 24 hours.

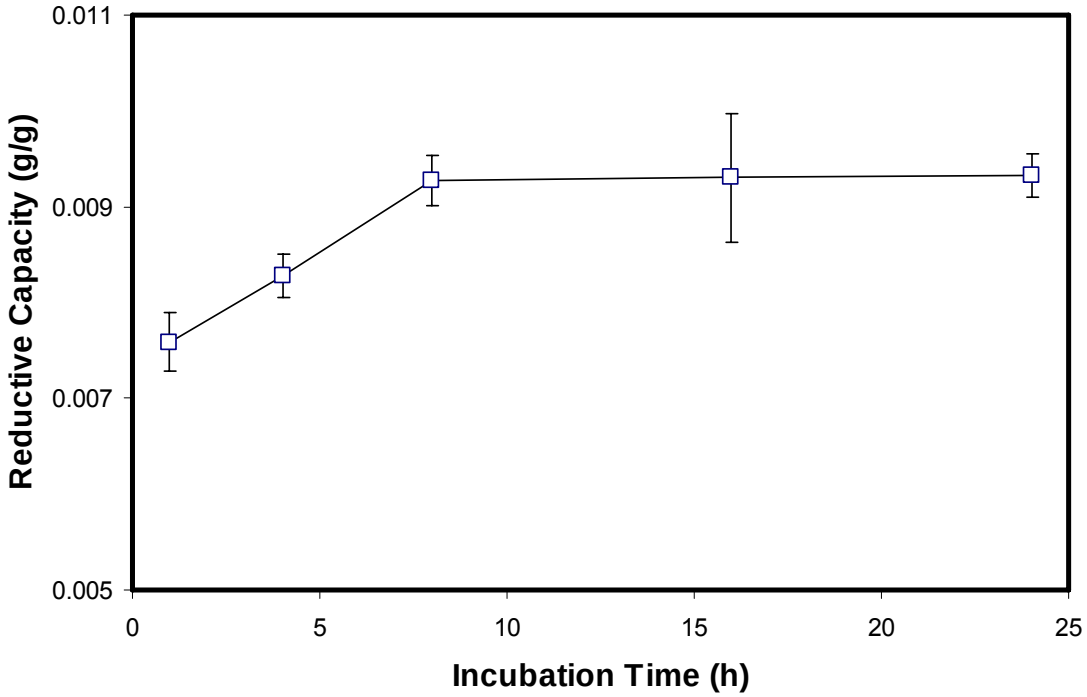

Fig. 28. The reductive capacity of CB at different incubation time. The solutions containing CB and Fe^{3+} ions were incubated for 1, 4, 8, 16 and 24 hours.

The results in Fig. 28 show that it takes 8 hours or less for CB to finish redox reaction with Fe^{3+}, and 82 % of reduction of Fe^{3+} ions takes place within first 1 hour of incubation. According to the results of CB, it is a reasonable conclusion that 16 hours is enough incubation time for nanomaterials to exert the reductive capacity to reduce Fe^{3+} ions.

5.3 Particle Separation

Since particles scatter and/or absorb light, remaining particles in the solution would hinder accurate absorbance measurement. Therefore, the particles remaining in the solutions were removed through either filtration or centrifugation after incubation. It was proved that both methods yield the same results as shown in Fig. 29.

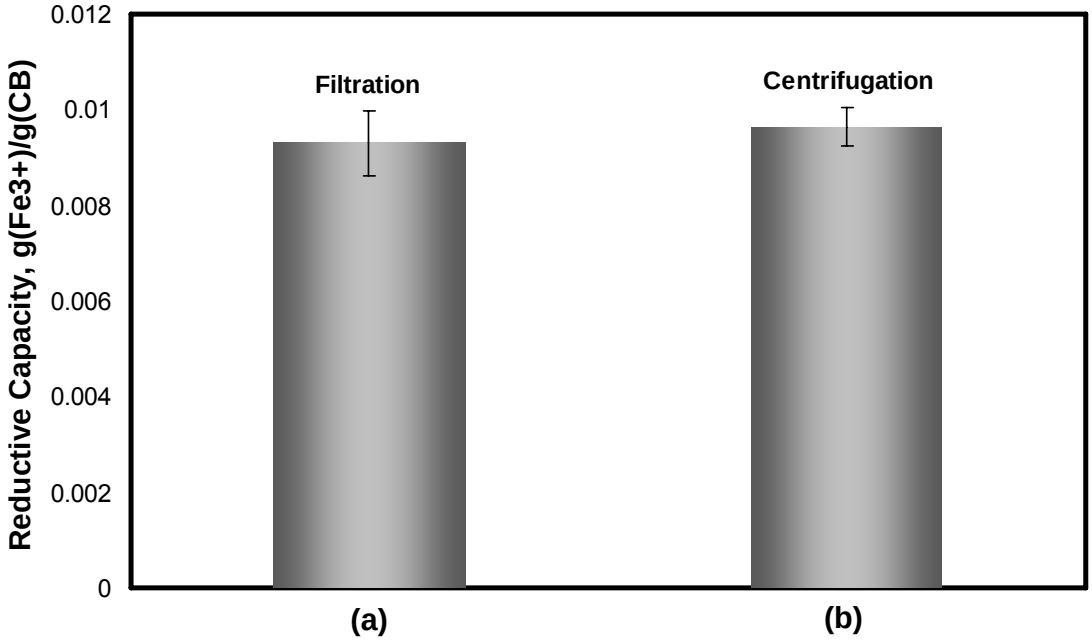

Fig. 29. The reductive capacity of CB measured using (a) Filtration, (b) Centrifugation.

The reductive capacity of CB using filtration and centrifugation is 9.3×10^{-3} and 9.6×10^{-3} g/g respectively. There is 4 % of difference between two results, however, this is statistically insignificant according to the t-test.

Filtration

A paper filter and plastic funnel were used for the filtration to separate the nanomaterials from incubated solution. The incubated solutions (75 ml each) were decanted into 100 ml volumetric flasks through the filter. The beakers used for incubation were rinsed with small amount of DI water (2~3 ml) several times, and DI water used to rinse the beakers was also filtered into the flasks so remaining Fe ions could be counted for the measurement. Finally, each flask was filled up to 100 ml mark with DI water through the paper filter in order to rinse the residual Fe ions on the paper filter into the flask. Requiring relatively short time, the filtration was used as prior method to centrifugation. And the filtration was effective for all carbon nanoparticles and nanotubes and amorphous silica but not for other metal oxides.

Centrifugation

A centrifuge was used to separate metal oxide because the paper filter could not filter nano-sized metal oxides. After dilution of incubated solutions to 100 ml, each solution was divided into two 50 ml centrifuge tubes. The tubes were balanced and centrifuged at 400 rpm for 8 minutes. As a result, metal oxides particles were precipitated on the bottom of the centrifuge tubes, and enough amount of the particle-free solution (approximately 80 ml) was obtained from two centrifuge tubes.

5.4 Optimal Conditions for Color Development and Absorbance Measurement

Effect of pH and Time for Color Development

As seen in Fig. 22, acidic condition is favorable for quick and steady color development of $Fe_2(SO_4)_3$. To keep the pH of the final solutions around 2, 0.25 ml of 20% sulfuric acid was added prior to adding phenanthroline. At pH around 2, intensity of the color reached its highest absorbance in 30 minutes, and once it reaches maximum color intensity, the absorbance does not change any more. Thus, the absorbance measurements were performed in 1 hour after the final solutions were made.

Effect of Order of Adding Chemicals and Photochemical Reduction

Since the order of adding reagent affect the absorbance results [55], the reagent were added in the order of 'incubated solution → hydroquinone → sulfuric aicd → phenanthroline → dilution with DI water'. It was reported that complex of Fe^{3+} and phenanthroline can be reduced to $[Fe(phen)_3]^{2+}$ even by room light and it may cause significant error in photometric method [56]. To investigate possible effects of photochemical reduction, 8.5 mg of $Fe_2(SO_4)_3$ was dissolved in 100 ml of DI water. A volume of 25 ml of this solution was put into three flasks ('A', 'B' and 'C'). Flask 'A' was diluted to 100 ml with DI water for method blank, and 0.25 ml of 20 % sulfuric acid was added into flask 'C'. Into flask 'B' and 'C', 10ml of 0.3 % phenanthroline was

added. Absorbance of each flask was read at various time points during a day with fluorescent lights on in the room. There was no direct sunlight coming into the room, and the fluorescent lights are bright enough to provide consistent light condition regardless of the weather. Absorbance of flask 'B' and 'C' were subtracted by absorbance of method blank (flask 'A').

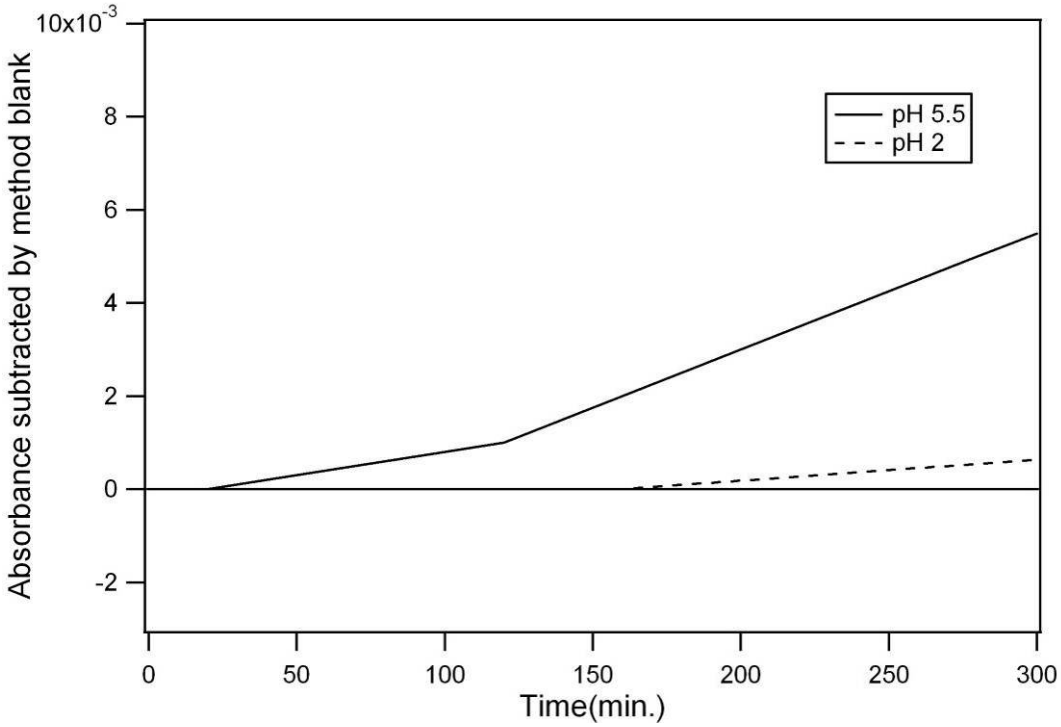

Fig. 30. Absorbance increase of $Fe_2(SO_4)_3$ solution with phenanthroline at different pH.

Apparently, the absorbance of $Fe_2(SO_4)_3$ solution with phenanthroline increased as time passed by, as seen in Fig. 30. However, the reaction is pH dependant, and in the standard method, pH of final solution (≈ 2) is so low that this effect can be neglected. Besides, even at higher pH (>5), reaction took place too slow to yield significant error in

1 hour. Even though it is not clear whether the increase of absorbance is due to photochemical reduction or not, it can be concluded the photochemical reduction does not interfere the standard method.

Other Factors Affecting Absorbance

All the factors which may affect the absorbance other than ferroin were investigated by measuring absorbances of reference solutions. The reference solutions were prepared so they have the same quantities of reagent as used in the final solutions. Both phenanthroline and hydroquinone do not affect the absorbance measurement showing zero absorbance of reference solutions. Although, $Fe_2(SO_4)_3$ reference solution has yellow color itself which may cause absorbance, Fig. 23 shows its contribution (absorbance 0.003) is negligible when 9 mg of $Fe_2(SO_4)_3$ is used. Fe impurities in the material would also contribute absorbance if Fe^{2+} ions are dissolved during incubation. The extractable Fe^{2+} from each material was determined as described in appendix C.

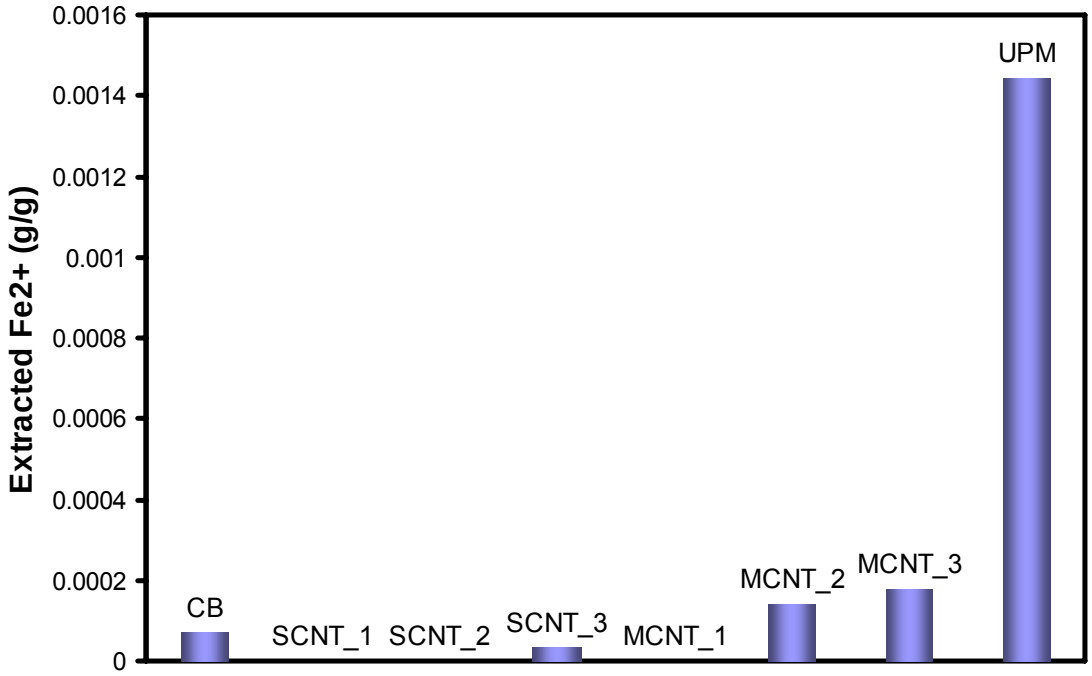

Fig. 31. Extracted Fe^{2+} (g/g) from the materials.

The results in Fig. 31 show UPM has a significant soluble Fe^{2+} and these results were taken into account for the reductive capacity anaylsis.

6. DISCUSSION

Oxidative stress, induced by reactive oxygen species (ROS) such as hydroxyl radical, has been evidenced as one of the main mechanisms of material's toxicity. When a material with significant reductive capacity co-exists with Fe^{3+} ions, Fe^{3+} ions would be reduced to Fe^{2+} by the material, and the reduced Fe^{2+} ions would generate hydroxyl radicals ($OH^{\cdot}$) by Fenton reaction.

$$Fe^{2+} + H_2O_2 \rightarrow Fe^{3+} + OH^{\cdot} + OH^{-}$$

Oxidation potential of $OH^{\cdot}$ is second highest (2.8 V) which is enough to cause serious oxidative stress initiating DNA damage and lipid peroxidation. Furthermore, Fe^{3+}, a byproduct of Fenton reaction, may be reduced again by the material, and this would make Fenton reaction keep taking place in a cycle. Considering the fact that Fe is one of the abundant materials in the air particulate matters and most frequently found impurity in commercial nanomaterials, this mechanism should be a plausible explanation.

Although, the reductive capacity was measured targeting only Fe^{3+} ions, the ability of materials to donate electrons may exert toxic effect by catalyzing ROS generations because electron donor is required in ROS formation such as superoxide and hydroxyl radical [57] as shown below.

$$O_2 + e^- \rightarrow O_2^-$$

$$H_2O_2 + e^- \rightarrow OH^- + OH^\cdot$$

Since the Fenton reaction is spontaneous, and the standard redox potential of Fe^{3+} is 0.77 V, the redox potential of hydrogen peroxide should be greater than 0.77 V. It means hydrogen peroxide has stronger tendency to take electrons, and it is easier to be reduced than Fe^{3+} ions are. Thus, if a material is able to reduce Fe^{3+} ions to Fe^{2+} ions by donating electrons, the material would also be able to reduce hydrogen peroxide and produce hydroxyl radicals.

$$Fe^{3+} + e^- \rightarrow Fe^{2+} \ (E_o = 0.77 \text{ V})$$

$$H_2O_2 + Fe^{2+} \rightarrow OH^- + OH^\cdot + Fe^{3+} \ (\text{spontaneous reaction, } E_o > 0)$$

$$\downarrow$$

$$H_2O_2 + e^- \rightarrow OH^- + OH^\cdot \ (E_o > 0.77 \text{ V})$$

Even though toxicity mechanisms of nanomaterials are not yet fully elucidated and still controversial, results of comparative toxicity studies are in accordance with the reductive capacity results in this study. CNTs are more toxic than metal oxides including SiO_2 and TiO_2 [58, 59], and C_{60} showed no toxicity while CNTs are significantly toxic where SCNT is more toxic than MCNT in terms of cell viability [60]. Among CNTs, acid-treated CNTs which have surface functional groups such as hydroxyl are more toxic than the pristine CNTs [61]. Considering the general trend of toxicity of materials used

this study accords closely with the reductive capacity results, the reductive capacity of a material may be an important factor for the toxicity of materials.

Anatase TiO_2 (Ti-A) and crystalline silica (Si-C) are generally known as toxic materials. Low or insignificant reductive capacities of these metal oxides indicate its ability to give or take electrons may not be the main reason for toxicity mechanisms of metal oxides. Besides, a toxicity study on TiO_2 particles found that surface area does not affect on its toxicity [62], suggesting the nature of metal oxide toxicity is not related to the surface reaction such as electron transfer.

7. SUMMARY AND CONCLUSION

A reproducible spectrophotometric method for determination of reductive capacity of nanomaterials was established as below.

- Iron(III) sulfate hydrate was selected for the initial ferric solution, and surfactant (Tween 20) was added for hydrophobic materials.
- Each measurement was performed at fixed Fe ratio of 0.066 ± 0.002 (30 ±0.2 mg of nanomaterials and 9 ± 0.2 mg of $Fe_2(SO_4)_3$) and at the same incubation conditions (16 hours at 37 ˚C).
- Particles were removed by filtration or centrifugation for reading absorbance, and absorbance was measured at pH 2 after 1 hour of color development.
- The reductive capacity of a material was determined as mean of reductive capacities of triplicate samples. The significance of the reductive capacity differences of each sample was assessed by the statistical tools (t-test and ANOVA).

The reductive capacities of carbon nanoparticles and nanotubes, metal oxides and standard reference materials were determined by the standardized method.

- CB has the highest reductive capacity (9.3×10^{-3} g/g) among tested materials, and 2 weeks of stirring caused decrease of reductive capacity by 34%.
- CNTs also have significant reductive capacity raging from 1.1×10^{-3} to 8.4×10^{-3} g/g depending on its type and surface functional groups; single-wall CNTs

generally have higher reductive capacity than multi-wall CNTs, and the one with OH groups shows higher reductive capacity than others. Graphitized CNTs are less reductive than pristine CNTs.

- Manually ground CNTs show increased reductive capacity which does not last long; 3 days of aging reduced its reductive capacity which has been increased by grinding.
- Fullerenes has different reductive capacity according to its surface functional groups; pristine C_{60} is not reductive towards Fe^{3+} while fullerenes with OH and H surface groups have reductive capacity of 7.7×10^{-3} and 1.8×10^{-3} g/g respectively.
- SRMs have a significant reductive capacity of 2.5×10^{-3} g/g.
- Metal oxides show relatively low reductive capacities in range of 0.9×10^{-4} ~ 5.4×10^{-4} g/g.

REFERENCES

1. Pouretedal HR, Shafiee B, Keshavarz MH. 2009. Simultaneous determination of trace amounts of thorium and zirconium using spectrophotometric partial least-squares calibration method. *Bulg Chem Commun* 41:230-235.

2. Agnihotri R, Agnihotri N, Kamal R, Mehta JR. 2008. 3-hydroxy-2-(3 '-methyl-2 '-thienyl)-4-oxo-4H-1-benzopyran as an analytical reagent for the spectrophotometric determination of tungsten(VI). *Asian J Chem* 20:4469-4476.

3. Kumar A, Sharma P, Chandel LK, Kalal BL. 2008. Synergistic extraction and spectrophotometric determination of palladium(II), iron(III), and tellurium(IV) at trace level by newly synthesized p-[4-(3,5-dimethylisoxazolyl)azophenylazo]calix(4)arene. *J Incl Phenom Macro* 61:335-342.

4. Ghaedi M, Shokrollahi A, Ekrampour F, Aghaei R. 2009. Sensitized spectrophotometric determination of trace amounts of copper(Ii) ion using diacetyl monooxime in surfactant media. *B Chem Soc Ethiopia* 23:337-345.

5. Hosseini MS, Hosseini-Bandegharaei A, Raissi H, Belador F. 2009. Sorption of Cr(VI) by Amberlite XAD-7 resin impregnated with brilliant green and its determination by quercetin as a selective spectrophotometric reagent. *J Hazard Mater* 169:52-57.

6. Nair AP, Christine J. 2009. 2-Hydroxy-4-n-propoxy-5-bromoacetophenone oxime as an analytical reagent for gravimetric determination of V(V). *E-J Chem* 6:303-307.

7. Waranyoupalin R, Wongnawa S, Wongnawa M, Pakawatchai C, Panichayupakaranant P, Sherdshoopongse P. 2009. Studies on complex formation between curcumin and Hg(II) ion by spectrophotometric method: A new approach to overcome peak overlap. *Cent Eur J Chem* 7:388-394.

8. Karimi MA, Mazloum-Ardakani M, Mashhadizadeh MH, Banifatemeh F. 2009. Simultaneous kinetic spectrophotometric determination of hydrazine and isoniazid using H-Point standard addition method and partial least squares regression in micellar media. *Croat Chem Acta* 82:729-738.

9. Tao H, Chen ZL, Li X, Yang YL, Li GB. 2008. Salicylate-spectrophotometric determination of inorganic monochloramine. *Anal Chim Acta* 615:184-190.

10. Burns DT, Mcalister JJ. 1981. Spectrophotometric determination of inorganic-phosphate in soil extracts by a single-solution non-reductive method. *Anal Chim Acta* 128:257-260.

11. Yu LY, Zhang XS, Dai SJ, Sun J, Yang YJ, Yu L, Xiao K. 2009. Simultaneous online visible detection of sulphide and chloride in tannery effluent by combination of fia and low pressure ion chromatography. *J Soc Leath Tech Ch* 93:250-254.

12. Amin AS, Gouda AAEF, El-Sheikh R, Zahran F. 2007. Spectrophotometric determination of gatifloxacin in pure form and in pharmaceutical formulation. *Spectrochim Acta A* 67:1306-1312.

13. Caglar S, Oztunc A. 2007. A sensitive spectrophotometric method for the determination of desloratadine in tablets. *J Aoac Int* 90:372-375.

14. Dincer Z, Basan H, Goger NG. 2003. Quantitative determination of ambroxol in tablets by derivative UV spectrophotometric method and HPLC. *J Pharmaceut Biomed* 31:867-872.

15. Nagata M, Noguchi Y, Ito H, Imanishi S, Sugiyama K. 2007. A simple spectrophotometric method for the estimation of alpha-carotene, beta-carotene and lycopene concentrations in carrot acetone extracts. *J Jpn Soc Food Sci* 54:351-355.

16. Onal A, Kepekci SE, Oztunc A. 2005. Spectrophotometric methods for the determination of the antidepressant drug paroxetine hydrochloride in tablets. *J Aoac Int* 88:490-495.

17. Singh DK, Verma R. 2009. Spectrophotometric determination of corticosteroids and its application in pharmaceutical formulation. *Oxid Commun* 32:678-684.

18. Squella JA, Sturm JC, Lenac R, Nunezvergara LJ. 1992. Polarographic and spectrophotometric determination of nimodipine in tablets. *Anal Lett* 25:281-292.

19. Verma KK, Jain A, Verma A, Chaurasia A. 1991. Spectrophotometric determination of ascorbic-acid in pharmaceuticals by background correction and flow-injection. *Analyst* 116:641-645.

20. White D, Abuhaidar G, Reinhold JG. 1958. Spectrophotometric measurement of bilirubin concentrations in the serum of the newborn by the use of a microcapillary method. *Clin Chem* 4:211-222.

21. Ahmed MJ, Roy UK. 2009. A simple spectrophotometric method for the determination of iron(II) aqueous solutions. *Turk J Chem* 33:709-726.

22. Balcerzak M, Tyburska A, Swiecicka-Fuchsel E. 2008. Selective determination of Fe(III) in Fe(II) samples by UV-spectrophotometry with the aid of quercetin and morin. *Acta Pharmaceut* 58:327-334.

23. Viollier E, Inglett PW, Hunter K, Roychoudhury AN, Van Cappellen P. 2000. The ferrozine method revisited: Fe(II)/Fe(III) determination in natural waters. *Appl Geochem* 15:785-790.

24. Pehkonen SO, Erel Y, Hoffmann MR. 1992. Simultaneous spectrophotometric measurement of Fe(Ii) and Fe(Iii) in atmospheric water. *Environ Sci Technol* 26:1731-1736.

25. Guo B, Kennedy IM. 2007. Gas-phase flame synthesis and characterization of iron oxide nanoparticles for use in a health effects study. *Aerosol Sci Tech* 41:944-951.

26. Karimi MA, Ardakani MM, Amiryan H. 2008. Simultaneous kinetic-spectrophotometric determination levodopa and carbidopa. *Asian J Chem* 20:2105-2114.

27. Guo L, Zhang Y, Li QM. 2009. A Novel Spectrophotometric method for the determination of levodopa with the detection system of potassium ferricyanide-Fe(III). *J Chin Chem Soc-Taip* 56:568-574.

28. El-Shiekh R, Amin AS, Zahran F, Gouda AA. 2007. Spectrophotometric determination of pipazethate hydrochloride in pure form and in pharmaceutical formulations. *J Aoac Int* 90:686-692.

29. Zarei AR, Afkhami A, Sarlak N. 2005. Simultaneous spectrophotometric determination of paracetamol and salicylamide in human serum and pharmaceutical formulations by a differential kinetic method. *J Aoac Int* 88:1695-1701.

30. Safavi A, Abdollahi H, Nezhad MRH. 2002. Indirect kinetic spectrophotometric determination of cobalt based on the redox reaction with iron(III) in the presence of 1,10-phenanthroline. *Spectrosc Lett* 35:681-688.

31. Szydlowska-Czerniak A, Dianoczki C, Recseg K, Karlovits G, Szlyk E. 2008. Determination of antioxidant capacities of vegetable oils by ferric-ion spectrophotometric methods. *Talanta* 76:899-905.

32. Berker KI, Guclu K, Tor I, Apak R. 2007. Comparative evaluation of Fe(III) reducing power-based antioxidant capacity assays in the presence of phenanthroline, batho-phenanthroline, tripyridyltriazine (FRAP), and ferricyanide reagents. *Talanta* 72:1157-1165.

33. Rodrigues CMP, Fan GS, Wong PY, Kren BT, Steer CJ. 1998. Ursodeoxycholic acid may inhibit deoxycholic acid-induced apoptosis by modulating mitochondrial transmembrane potential and reactive oxygen species production. *Mol Med* 4:165-178.

34. Babich H, Borenfreund E. 1990. Applications of the neutral red cytotoxicity assay to invitro toxicology. *Atla-Alternatives to Laboratory Animals* 18:129-144.

35. Soderberg TA, Johansson A, Gref R. 1996. Toxic effects of some conifer resin acids and tea tree oil on human epithelial and fibroblast cells. *Toxicology* 107:99-109.

36. Kladna A, Aboul-Enein HY, Kruk I. 2003. Enhancing effect of melatonin on chemiluminescence accompanying decomposition of hydrogen peroxide in the presence of copper. *Free Radical Bio Med* 34:1544-1554.

37. Codina JC, Cazorla FM, Perez-Garcia A, de Vicente A. 2000. Heavy metal toxicity and genotoxicity in water and sewage determined by microbiological methods. *Environmental Toxicology and Chemistry* 19:1552-1558.

38. Stohs SJ, Bagchi D. 1995. Oxidative mechanisms in the toxicity of metal-ions. *Free Radical Bio Med* 18:321-336.

39. Valko M, Morris H, Cronin MTD. 2005. Metals, toxicity and oxidative stress. *Curr Med Chem* 12:1161-1208.

40. Huang XD, Atwood CS, Hartshorn MA, Multhaup G, Goldstein LE, Scarpa RC, Cuajungco MP, Gray DN, Lim J, Moir RD, Tanzi RE, Bush AI. 1999. The A beta peptide of Alzheimer's disease directly produces hydrogen peroxide through metal ion reduction. *Biochemistry-Us* 38:7609-7616.

41. Guo B, Zebda R, Drake SJ, Sayes CM. 2009. Synergistic effect of co-exposure to carbon black and Fe2O3 nanoparticles on oxidative stress in cultured lung epithelial cells. *Part Fibre Toxicol* 6:-.

42. Arts JHE, Muijser H, Duistermaat E, Junker K, Kuper CF. 2007. Five-day inhalation toxicity study of three types of synthetic amorphous silicas in Wistar rats and post-exposure evaluations for up to 3 months. *Food Chem Toxicol* 45:1856-1867.

43. Nishi K, Morimoto Y, Ogami A, Murakami M, Myojo T, Oyabu T, Kadoya C, Yamamoto M, Todoroki M, Hirohashi M, Yamasaki S, Fujita K, Endo S, Uchida K, Yamamoto K, Nakanishi J, Tanaka I. 2009. Expression of cytokine-induced neutrophil chemoattractant in rat lungs by intratracheal instillation of nickel oxide nanoparticles. *Inhal Toxicol* 21:1030-1039.

44. Ross P, DeSwart R, Addison R, VanLoveren H, Vos J, Osterhaus A. 1996. Contaminant-induced immunotoxicity in harbour seals: Wildlife at risk? *Toxicology* 112:157-169.

45. Newcombe DT, Cardwell TJ, Cattrall RW, Kolev SD. 1999. An optical redox chemical sensor based on ferroin immobilised in a Nafion (R) membrane. *Anal Chim Acta* 401:137-144.

46. Rose HE. 1952. Breakdown of the Lambert-Beer law. *Nature* 169:287-288.

47. Kung KH, Mcbride MB. 1988. Electron-transfer processes between hydroquinone and iron-oxides. *Clays and Clay Minerals* 36:303-309.

48. Fu RW, Zeng HM, Lu Y. 1994. Studies on the mechanism of the reaction of activated carbon-fibers with oxidants. *Carbon* 32:593-598.

49. Ting JH, Li TL, Hong YC. 2006. Dependence of field emission properties of carbon nanotube films on their graphitization. *Journal of Vacuum Science & Technology B* 24:1794-1798.

50. Fenoglio I, Greco G, Tornatis M, Muller J, Rayrnundo-Pinero E, Beguin F, Fonseca A, Nagy JB, Lison D, Fubini B. 2008. Structural defects play a major role in the acute lung toxicity of multiwall carbon nanotubes: Physicochemical aspects. *Chem Res Toxicol* 21:1690-1697.

51. Jorio A, Saito R, Dresselhaus G, Dresselhaus MS. 2004. Determination of nanotubes properties by Raman spectroscopy. *Philosophical Transactions of the Royal Society a-Mathematical Physical and Engineering Sciences* 362:2311-2336.

52. Jensen MS, Bainton DF. 1973. Temporal Changes in Ph within Phagocytic vacuole of polymorphonuclear neutrophilic leukocyte. *J Cell Biol* 56:379-388.

53. Koch S, Ackermann G, Lindner P. 1992. Application of redox reactions in spectrophotometry .2. detection and spectrophotometric determination of Phenolic-compounds with the iron(III)/1,10-phenanthroline complex. *Talanta* 39:693-696.

54. Yasuko N, Masahir O N, Atsushi N, Hideo T, Masahiro K. 2001. Hydroxyl radical generation induced by ultra-sonication: An ESR study. *Nippon Kagakkai Koen Yokoshu* 79th:1.

55. Tamura H, Goto K, Yotsuyan.T, Nagayama M. 1974. Spectrophotometric dtermination of iron(II) with 1,10-phenanthroline in presence of large amounts of iron(III). *Talanta* 21:314-318.

56. Stucki JW, Anderson WL. 1981. The quantitative assay of minerals for Fe2+ and Fe3+ using 1,10-phenanthroline .1. Sources of variability. *Soil Sci Soc Am J* 45:633-637.

57. Munday R. 1988. Generation of superoxide radical, hydrogen-peroxide and hydroxyl radical during the autoxidation of N,N,N',N'-Tetramethyl-Para-Phenylenediamine. *Chemico-Biological Interactions* 65:133-143.

58. Simon-Deckers A, Gouget B, Mayne-L'Hermite M, Herlin-Boime N, Reynaud C, Carriere M. 2008. In vitro investigation of oxide nanoparticle and carbon nanotube toxicity and intracellular accumulation in A549 human pneumocytes. *Toxicology* 253:137-146.

59. Lam CW, James JT, McCluskey R, Arepalli S, Hunter RL. 2006. A review of carbon nanotube toxicity and assessment of potential occupational and environmental health risks. *Crit Rev Toxicol* 36:189-217.

60. Cheng C, Porter AE, Muller K, Koziol K, Midgley P, Wallend M. 2009. Imaging carbon nanoparticles and related cytotoxicity. In Kenny L, ed, *10th International Symposium on Inhaled Particles*. Iop Publishing Ltd, Dirac House, Temple Back, Bristol BS1 6BE, England, Sheffield, England.

61. Bottini M, Bruckner S, Nika K, Bottini N, Bellucci S, Magrini A, Bergamaschi A, Mustelin T. 2006. Multi-walled carbon nanotubes induce T lymphocyte apoptosis. *Toxicol Lett* 160:121-126.

62. Warheit DB, Webb TR, Sayes CM, Colvin VL, Reed KL. 2006. Pulmonary instillation studies with nanoscale TiO2 rods and dots in rats: Toxicity is not dependent upon particle size and surface area. *Toxicological Sciences* 91:227-236.

APPENDIX A

SAMPLE TREATMENTS

Grinding and aging of CNTs

(a) The mortar and pestle are cleaned with Isopropyl alcohol and dried before use.

(b) 200 mg of CNT is weighted and placed in the pestle.

(c) The CNT is manually ground by a mortar for 20 minutes and transferred to a vial followed by shaking to mix ground CNT.

(d) 90 mg of ground CNT is immediately used for reductive capacity measurement.

(e) The rest of ground CNT is dispersed on a weighing paper and left in ambient air for 3 days for another reductive capacity measurement.

Oxidization of CB and Soot-A

(a) 90 mg of CB or Soot-A is weighted and placed in a jar.

(b) 200 ml of DI water is added and stirred by a magnetic on a stir plate at room temperature (20 ± 3˚C). The cap of the jar should be loosen so that air can diffuse into the jar.

(c) After 2 weeks of stirring, oxidized material is analyzed as a form of suspension.

APPENDIX B

SYNTHESIS OF TiO_2 (ANATASE)

Anatase TiO_2 nanoparticles were synthesized in a H_2/O_2 flame using titanium(IV) i-propoxide as a precursor. The flame apparatus for TiO_2 synthesis is schematically shown in Fig. 32.

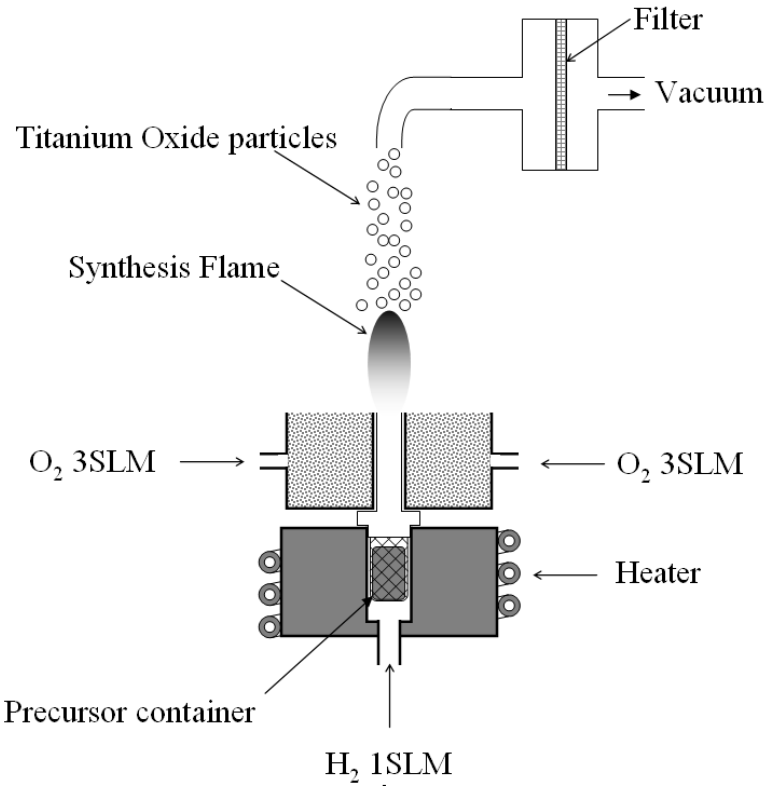

Fig. 32. The schematic of flame apparatus for TiO_2 synthesis.

1 Standard Liter per Minute (SLM) of H_2 and 6 SLM of O_2 were used as fuel gas and oxidizer, respectively. Even though the vapor pressure of titanium(IV) isopropoxide is high enough to be vaporized at room temperature (25 ˚C), a heater was installed to help vaporizing precursor by increasing temperature up to 200 ˚C. The precursor container was designed to hold approximately 0.5 ml of titanium(IV) isopropoxide in the heater so that H_2 gas could carry vaporized precursor to the outlet. The vapor of precursor in H_2 gas was burned and formed anatase TiO_2 nanoparticle in the synthesis flame. The nanoparticles collected on the alumina filter by vacuum were scraped off and stored in a vial. The synthesis was repeated until 200 mg of TiO_2 was obtained for reductive capacity assay.

APPENDIX C

DETERMINATION OF EXTRACTABLE Fe^{2+} IN THE MATERIALS

(a) 30 mg of a material is put into a 200 ml beaker and suspended in 75 ml of DI water.

(b) 0.02 ml of 5 % sulfuric acid is added to make pH around 3.5 which is the same pH of incubation solution of the standard method using 9 mg of $Fe_2(SO_4)_3$.

(c) The beaker is incubated in the same conditions as used in the standard method (16 hours at 37 ˚C).

(d) After incubation, the amount of Fe^{2+} leached from 30 ± 0.2 mg of the sample is determined by the same spectrophotometric technique used in the standard method.

APPENDIX D

CONVERSION OF ABSORBANCE LIMIT TO MEASUREMENT UNCERTAINTY

(a) The spectrophotometer has an absorbance limit of 0.002

(b) Based on the calibration curve in Fig. 4, this absorbance limit (0.002) corresponds to 0.0106 mg/L of Fe^{2+} concentration in final solution. (0.002 / 0.1893 = 0.0106 mg/L)

(c) In 100 ml of the final solution, 25 ml of the original solution is contained, thus, Fe^{2+} concentration of the original solution is 4 times higher than that of the final solution. (0.0106 × 4 = 0.0423 mg/L)

(d) Since, the volume of the original solution is 100 ml, the mass of Fe^{2+} in the original solution is 0.0042 mg. (0.0423 × 100 /1000 ≈ 0.0042 mg)

(e) 0.0042 mg of Fe^{2+} yields 1.4×10^{-4} g/g of reductive capacity when 30 mg of a material is used. (0.0042 / 30 = 1.4×10^{-4} g/g)

VITA

Name:	Wonjoong Hwang
Address:	Texas A&M University, Department of Mechanical Engineering, 3123 TAMU, College Station, TX 77843-3123
Email Address:	c14945@hamail.net
Education:	B.E., Mechanical Engineering, Korea Military Academy in South Korea, 2005
	M.S., Mechanical Engineering, Texas A&M University, 2010